1 # Sources of organic aerosols in eastern China: A modeling study

2 # with high-resolution intermediate-volatility and semi-volatile

3 # organic compound emissions

4 Jingyu An[1], Cheng Huang[1*], Dandan Huang[1], Momei Qin[2,1], Huan Liu[3], Rusha Yan[1], Liping

5 Qiao[1], Min Zhou[1], Yingjie Li[1], Shuhui Zhu[1], Qian Wang[1], Hongli Wang[1]

6 1. State Environmental Protection Key Laboratory of the Formation and Prevention of Urban Air

7 Pollution Complex, Shanghai Academy of Environmental Sciences, Shanghai 200233, China

8 2. Jiangsu Key Laboratory of Atmospheric Environment Monitoring and Pollution Control,

9 Collaborative Innovation Center of Atmospheric Environment and Equipment Technology,

10 Nanjing University of Information Science & Technology, Nanjing 210044, China

11 3. State Key Joint Laboratory of Environment Simulation and Pollution Control, School of

12 Environment, Tsinghua University, Beijing 100084, China

13 **Abstract:** Organic aerosol (OA) makes up a substantial fraction of atmospheric

14 particulate matter that exerts tremendous impacts on air quality, climate, and human

15 health. Yet current chemical transport models fail to reproduce both the concentrations

16 and temporal variations of OA, especially the secondary organic aerosol (SOA),

17 hindering the identification of major contribution sources. One possibility is that

18 precursors that are not yet included in the model exist, and intermediate-volatility and

19 semi-volatile organic compounds (I/SVOCs) are advocated to be one of them. Herein,

20 we established a high-resolution emission inventory of I/SVOCs and by incorporating

21 it into the CMAQ model, concentrations, temporal variations, and spatial distributions

22 of POA and SOA originated from different sources in the Yangtze River Delta (YRD)

23 region of China were ~~successfully~~ simulated. Compared with the comprehensive

24 observation data obtained in the region, i.e., volatile organic compounds (VOCs),

25 organic carbon (OC), primary organic aerosol (POA) and SOA, significant model

* Correspondence to C. Huang (huangc@saes.sh.cn)

improvements in the simulations of different OA components were demonstrated. Furthermore, spatial and seasonal variations of different source contributions to OA production were identified. We found cooking emissions are predominant sources of POA in the densely populated urban area of the region. I/SVOC emissions from industrial sources are dominant contributors to the SOA formation, followed by those from mobile sources. While the former concentrated in eastern, central, and northern YRD, the latter mainly focused on the urban area. Our results indicate that future control measures should be specifically tailored on intraregional scale based on the different source characteristics to achieve the national goal of continuous improvement in air quality. In addition, local source profiles and emission factors of I/SVOCs as well as SOA formation mechanisms in model framework are urgently needed to be updated to further improve the model performance and thus the accuracy of source identifications.

Key words: semi-volatile and intermediate volatility organic compounds; secondary organic aerosol; emission inventory; source contribution; model simulation

1. Introduction

Organic aerosol (OA) contributes a large fraction (20 to 90%) of atmospheric submicron aerosol (Zhang et al., 2007; Jimenez et al., 2009) and has negative impacts on air quality, climate (Shrivastava et al., 2017), and human health (Nault et al., 2021). OA is composed of primary organic aerosol (POA) directly emitted from fossil fuel combustion, biomass burning, and other sources, as well as secondary organic aerosol (SOA) formed through the atmospheric oxidation of gas-phase species emitted from a wide range of biogenic and anthropogenic sources (Hallquist et al., 2009). Understanding and identifying the origins of OA is therefore important for elucidating their health and climate effects and establishing effective mitigation policies. However, OA is a dynamic system driven by the gas-particle partitioning of organic vapors and particulate organic material, i.e. POA and SOA, and continuously evolves upon atmospheric oxidation (Robinson et al., 2007; Donahue et al., 2009; Zhao et al., 2013; Jathara et al., 2014). Constraints in their precursors and further source identification

54   have been facing great challenges.

55   Great efforts have been made in the identification of OA sources through source

56   apportionment of the measured OA components, such as positive matrix factorization

57   (PMF), chemical mass balance (CMB) model or multilinear engine (ME-2). The

58   Aerodyne high-resolution time-of-flight aerosol mass spectrometer (AMS), has been

59   proven to be a powerful tool in quantification and chemical characterization of different

60   OA components in real-time. Coupled with PMF analysis, AMS measurements allow

61   for the deconvolution of physically meaningful OA factors. Commonly retrieved factors

62   include three POA sources, i.e. hydrocarbon-like OA (HOA) related to fossil fuel

63   combustion, biomass burning OA (BBOA), and cooking-related OA (COA), as well as

64   two SOA components, i.e. less oxidized oxygenated OA (LO-OOA) and more oxidized

65   oxygenated OA (MO-OOA) (Hayes et al., 2013; Crippa et al., 2014; Sun et al., 2014;

66   Li et al., 2017). Combining offline AMS and radiocarbon (^{14}C) measurements, Huang

67   et al. (2014) also identified the contributions of fossil and non-fossil sources to SOA.

68   Attempts have been made in subsequent studies by coupling the AMS measurement

69   with a suite of comprehensive and collocated SOA tracer measurements to distinguish

70   biogenic and major anthropogenic SOA sources, such as traffic and cooking emission

71   (Xu et al., 2015; Zhang et al., 2018; Zhu et al., 2020; Huang et al., 2021a). However,

72   due to the complex OA composition and variety of emission sources, further

73   deconvolution on the contributions of different sources to OA production is challenging.

74   Besides field measurements, air quality model is another widespread technique,

75   which advantages in regional-scale OA source apportionment with higher temporal and

76   spatial resolution. However, the model simulated SOA concentration still has large

77   gapsis substantially lower than that measured in the atmosphere. On one hand, this is

78   limited by the model treatment, where multiple-generation oxidation of organic vapors

79   is not included. The volatility basis set (VBS) scheme is therefore developed, which

80   lumps organic precursors as well as their oxidation products into different volatility bins.

81   Upon atmospheric aging, the volatility of these compounds evolves due to the processes

82   such as functionalization and fragmentation, which can be accounted for in the models

83   by shifting the volatility bins of these compounds (Donahue et al., 2006). It has been

84   widely reported that coupling VBS scheme with air quality models can improve the

85   model performance on SOA simulation (Tsimpidi et al., 2010; Koo et al., 2014; woody

86   et al., 2016; Zhao et al., 2016a; Yang et al., 2019). However, there are still some

87   shortcomings in the modeling of OA with the VBS, for example the lack of

88   representation of the hydrophilic properties of OA, which assumes SOA condenses onto

89   an organic phase, whereas SOA may also condense on an aqueous phase (Kim et al.,

90   2011). Another important constraint is On the other hand, the gaps are still not closed

91   mainly due to the underestimation missing of intermediate-volatility organic

92   compounds (IVOCs) and semi-volatile organic compounds (SVOCs) emissions in the

93   models, which potentially have substantial contributions to SOA budget owing to their

94   high SOA yields (Presto et al., 2009; Tkacik et al., 2012; Zhao et al., 2014; Liggio et

95   al., 2016). IVOCs refer to organic compounds with effective saturation concentrations

96   (C*) between 10^3 to 10^6 μg·m^{-3} at 298 K and 1 atm, while SVOCs refer to organic

97   compounds with C* between 10^{-1} to 10^3 μg·m^{-3} at 298 K and 1 atm (Robinson et al.,

98   2007).

99   I/SVOC emission inventories have been developed and applied into air quality

100   models over the past decade. Most of them were estimated by applying different scaling

101   factors based on their relationship with POA, volatile organic compounds (VOCs), or

102   some proxies like naphthalene (Pye and Seinfeld, 2010; Shrivastava et al., 2011; Jathar

103   et al., 2017; Wu et al., 2019, 2021; Li et al., 2020, 2022; Ling et al., 2022). Yet in

104   practice, a same scaling factor was applied to most of the sources in previous studies

105   due to the lack of measurements on I/SVOC emission factors. For example, except

106   biomass burning (0.75–1.5), Wu et al. (2019) utilized scaling factors of 8–30 for all of

107   the other emission source categories, which was estimated based on the measurements

108   of on-road mobile source. Li et al. (2020) assumed scaling factors of 1.5 for on-road

109   mobile source, and 0.34–1.5 for the other sources, such as industrial and residential

sources, which were much lower than the estimations in Wu et al. (2020). Huang et al. (2021) have tried emission factor method to quantify the I/SVOC emissions, yet the results were 60% lower than the scaling factor method, far from catching the measured amount of SOA. Obviously, roughly estimating I/SVOC emissions using one or two emission profiles as surrogates for all emission sources will create large uncertainties.

~~However, due to the vast number of different I/SVOC components with low volatility (C^* of 10^{-1} to 10^6 $\mu g \cdot m^{-3}$) and concentrations, qualitative and quantitative characterization of I/SVOCs in molecular level are difficult.~~ Recent studies have successively determined the volatility distribution, chemical composition, and emission factors of I/SVOCs from mobile sources, including gasoline and diesel vehicles, non-road diesel machinery, marine vessel, and aircraft (Presto et al., 2011; Cross et al., 2013; Zhao et al., 2015, 2016b; Huang et al., 2018; Qi et al., 2019; Drozd et al., 2019). I/SVOC emission profiles have been reported for nonmobile-sources as well, including coal combustion, wood-burning, cooking, fuel evaporation, and industrial and residential volatile chemical products (Huffman et al., 2009; Gentner et al., 2012; May et al., 2013; Koss et al., 2018; McDonald et al., 2018; Cai et al., 2019; Drozd et al., 2021)~~. Most of these reported emission profiles have been released in SPECIATE 5.1 (US EPA, 2021)~~, making the quantification of I/SVOC emissions and their involvement in air quality models possible.

In China, SOA has been emerging as an important contributor to air pollution. Field observations reveal that OA contributes significantly~~dominates~~ (30%) the $PM_{2.5}$ concentrations in most parts of China (Tao et al., 2017; Liu et al., 2018), among which the SOA contributes up to 80% of OA during haze pollution (Huang et al., 2014; Ming et al., 2017; Li et al., 2021). SOA formation in China has already been examined in several modeling studies. They found that by considering the POA aging and I/SVOCs oxidation in the models, which is realized by the coupling of VBS scheme, the formation and evolution of SOA can be much better simulated compared to the results of the two-product SOA modeling framework (Zhao et al., 2016a; Wu et al., 2019; Li

et al., 2020; Yao et al., 2020; Huang et al., 2021). Chang et al. (2022) developed a full-volatility organic emission inventory with source-specific I/SVOC emission profiles for China, which have greatly improved the model performance on SOA concentrations. However, large gaps still exist between the observed and modeled SOA. Studies on high-resolution I/SVOC emission inventory for more specific sources are highly needed. ~~large uncertainties still exist in the estimation of I/SVOC emissions used in previous modeling studies, which has essential impacts on model performance. Theoretically, the I/SVOC emissions can be obtained quantitatively by applying different scaling factors to POA emissions from different sources. Yet in practice, a same scaling factor was applied to most of the sources in previous studies due to the lack of measurements on I/SVOC emission factors. For example, except biomass burning (0.75–1.5), Wu et al. (2019) utilized scaling factors of 8–30 for all of the other emission source categories, which was estimated based on the measurements of on-road mobile source. Li et al. (2020) assumed scaling factors of 1.5 for on-road mobile source, and 0.34–1.5 for the other sources, such as industrial and residential sources, which were much lower than the estimations in Wu et al. (2020). Huang et al. (2021) have tried emission factor method to quantify the I/SVOC emissions, yet the results were 60% lower than the scaling factor method, far from catching the measured amount of SOA.~~

~~Beyond the aforementioned uncertainties, another obstacle is that I/SVOC emission profiles have not been taken into account in previous studies. It should be noted that volatility and chemical composition of I/SVOC emissions vary by source category (Lu et al., 2018), which matters in model simulation because different I/SVOC components are of different SOA yields. For example, the SOA yields of *n*-alkanes increase with increasing carbon number (Presto et al., 2010) and for a given volatility bin, the aromatics usually have higher SOA yields than the alkanes (Lim and Ziemann, 2009; Tkacik et al., 2012). In a recent study, Lu et al. (2020) compiled new emission profiles for I/SVOCs based on the existing mobile-source emission data and incorporated them into an updated version of the Community Multiscale Air Quality~~

166   model version 5.3 (CMAQ v5.3) to investigate their contributions to SOA formation.

167   Their results indicated that mobile-source related I/SVOC emissions produced almost

168   as much SOA as traditional precursors such as single-ring aromatics in southern

169   California and suggested that the potential contributions of nonmobile-source I/SVOC

170   emissions were nonnegligible to SOA formation (Lu et al., 2020).

171   In this study, taking the Yangtze River Delta (YRD) region, including Jiangsu,

172   Zhejiang, Anhui provinces and Shanghai city, as a pilot, we established a high-

173   resolution source specific I/SVOC emission inventory. We then applied the newly

174   established inventory into CMAQ v5.3 to evaluate the contributions of I/SVOC

175   emissions to SOA formation by comparing the results with the observation data

176   collected in the region. Furthermore, we also run the model in different scenarios to

177   quantify the seasonal contributions of different sources to POA and SOA formation in

178   the YRD region.

179   **2. Materials and methods**

180   2.1 I/SVOC emission inventoryestimates

181   I/SVOCs commonly exist in both gas- and particle-phase in the atmosphere.

182   Previous studies usually used POA scaling factors to estimate the I/SVOC emissions,

183   which may lead to large uncertainties in the estimation of gas-phase organic compound-

184   dominated sources, like oil refinery, chemical production, and industrial solvent-use.

185   Herein, we compiled both gas-phase I/SVOCs (I/SVOCs-G) and particle-phase

186   I/SVOCs (I/SVOCs-P) emission inventories and incorporate them into the model.

187   Detailed process of the inventories is as follows.

188   I/SVOCs-G emissions for each specific source were estimated by the ratios of total

189   I/SVOC components to VOC components (I/SVOCs-to-VOCs). Similarly, I/SVOCs-P

190   emissions were estimated by the ratios of total particle-phase I/SVOC components to

191   POA (I/SVOCs-to-POA). On this basis, we further determined the source profiles of

192   I/SVOCs for each source. The I/SVOCs-G emissions were distributed into four lumped

193   aliphatic IVOC bins across the volatility basis set from $C^*=10^3$ to 10^6 $\mu g \cdot m^{-3}$, two

194 ~~aromatic IVOC bins with the C*=10⁵ and 10⁶ μg·m⁻³, and four lumped SVOC bins with~~

195 ~~C* from 10⁻¹ and 10² μg·m⁻³. The I/SVOCs-P emissions were distributed into five bins~~

196 ~~spanning C* from 10⁻¹ and 10³ μg·m⁻³.~~

197 (1) Source classification: To refine the I/SVOC emissions from different sources,

198 we divided the sources into five major categories and then further grouped them into

199 21 sub-categories. The major categories include ~~In this study, we first divided the~~

200 ~~sources into five categories, including~~ industrial process sources, industrial solvent-use

201 sources, mobile sources, residential sources, and agricultural sources. As shown in

202 Table S1, the ~~, and then further grouped them into 21 sub-categories. For example,~~

203 industrial process sources include the sectors such as oil refinery, chemical production,

204 and pulp and paper production; Industrial solvent-use sources include textile, leather

205 tanning, timber processing, and various industrial volatile chemical products use;

206 Mobile sources include gasoline and diesel vehicle emissions, fuel evaporation, diesel

207 machinery, marine vessel, and aircraft; Residential sources include coal combustion,

208 residential solvent-use, and cooking emissions; Agricultural source is specifically

209 referred to biomass burning in household stoves, and open burning was not included in

210 this study.

211 (2) Emission estimation: I/SVOCs-G emissions for each specific source were

212 estimated by the ratios of total I/SVOC components to anthropogenic VOC (AVOC)

213 components (I/SVOCs-to-VOCs). Similarly, I/SVOCs-P emissions were estimated by

214 the ratios of total particle-phase I/SVOC components to POA (I/SVOCs-to-POA). The

215 I/SVOCs-G-to-VOCs and I/SVOCs-P-to-POA ratios for each source were determined

216 according to their fractions of total I/SVOC species in VOC and POA emissions. Then

217 we grouped different I/SVOC species into lumped I/SVOC bins based on their C* to

218 determine the volatility distributions of each source. The I/SVOCs-G emissions were

219 distributed into four lumped aliphatic IVOC bins across the volatility basis set from

220 C*=10³ to 10⁶ μg·m⁻³, two aromatic IVOC bins with the C*=10⁵ and 10⁶ μg·m⁻³, and

221 four lumped SVOC bins with C* from 10⁻¹ and 10² μg·m⁻³. The I/SVOCs-P emissions

were distributed into five bins spanning C* from 10^{-1} and 10^3 μg·m^{-3}. Source profiles of I/SVOC species for different sources were referenced from the results in previous studies. Table S1 and S2 show the I/SVOCs-G-to-VOCs and I/SVOCs-P-to-POA ratios for each specific source and their references. For industrial process, industrial solvent-use, and residential solvent-use sources, only I/SVOCs-G emissions were considered. Their I/SVOCs-G-to-VOCs ratios and emission profiles were derived from the latest version of SPECIATE 5.1 database (US EPA, 2021). For gasoline and diesel vehicles, the I/SVOCs-G-to-VOCs and I/SVOCs-P-to-POA ratios and emission profiles were referenced from a new mobile-source parameterization recommended by Lu et al. (2020). Those of diesel machinery, marine vessel, and residential coal combustion were determined by recent measurement results in China (Qi et al., 2019; Huang et al., 2018; Cai et al., 2019). The I/SVOCs-G-to-VOCs ratios and profiles of cooking and biomass burning emissions were derived from SPECIATE 5.1 database, while their particle-phase ratios and profiles were referenced from two previous studies (May et al., 2013; Louvaris et al., 2017). Table S1 and S2 show the I/SVOCs-G-to-VOCs and I/SVOCs-P-to-POA ratios and their emission profiles of each specific source. The base emissions of AVOCs and POA (See Table S3) were taken from a high-resolution emission inventory for the year of 2017 developed in our previous study (An et al., 2021).

(3) Model input: Before being input into the model, the estimated I/SVOC-G and I/SVOC-P emissions were summed and then redistributed according to their phase equilibrium under the actual atmospheric state. The formula of phase equilibrium is shown in Equation (1).

$$F_{\mathrm{p}} = \frac{c_{\mathrm{OA}}}{c_{\mathrm{OA}}+c^*} \tag{1}$$

Where, F_{p} is the fraction of particle-phase I/SVOC emissions for each volatility bin. c_{OA} represents the OA concentration in the atmosphere. We assumed it to be 10 μg·m^{-3} in this study. C^* is the effective saturation concentration of each volatility bin. After redistribution, For gasoline and diesel vehicles, the I/SVOCs-G-to-VOCs and I/SVOCs-P-to-POA ratios and their emission profiles were derived from a new mobile-

250 ~~source parameterization recommended by Lu et al. (2020). Those of diesel machinery,~~

251 ~~marine vessel, and residential coal combustion were determined by recent measurement~~

252 ~~results in China (Qi et al., 2019; Huang et al., 2018; Cai et al., 2019). The emission~~

253 ~~profiles of other sources were derived from the latest version of SPECIATE 5.1 database~~

254 ~~(US EPA, 2021). Table S1 and S2 respectively show the I/SVOCs-G-to-VOCs and~~

255 ~~I/SVOCs-P-to-POA ratios and their emission profiles for specific sources. The base~~

256 ~~emissions of anthropogenic VOCs (AVOCs) and POA (See Table S3) were taken from~~

257 ~~a high-resolution emission inventory for the year of 2017 developed in our previous~~

258 ~~study (An et al., 2021). Tt~~he I/SVOCs emissions for each source category were

259 allocated into 4 km × 4 km grids and hourly temporal profiles using the same method

260 as the criteria pollutants.

261 2.2 Model configuration

262 We used Community Modeling and Analysis System (CMAQ version 5.3.2) to

263 simulate the concentrations of air pollutants. The domain of the simulation is presented

264 in Figure 1. The simulations were conducted for three nested grids with horizontal

265 resolution of 36 km (D1), 12 km (D2) and 4 km (D3), respectively. D1 covers most of

266 China and the surrounding countries including Japan and South Korea; D2 covers

267 eastern China and D3 covers the entire YRD region and its surrounding land and waters.

268 Meteorological fields were provided by the Weather Research and Forecasting

269 (WRF version 3.7) model with 27 vertical layers extending to the tropopause (100 hpa).

270 The initial and boundary conditions (ICs, BCs) in the WRF were based on the 1° × 1°

271 reanalysis data from the National Centers for Environmental Prediction Final Analysis

272 (NCEP-FNL). Physical options used in the WRF simulation are listed in Table S4.

273 The Sparse Matrix Operator Kernel Emissions (SMOKE,

274 https://cmascenter.org/smoke) model was applied to process emissions for input to

275 CMAQ. CMAQ version 5.3.2 (https://cmascenter.org/cmaq/) was used to simulate

276 atmospheric pollutants concentrations. ICs and BCs of D1 domain are based on a Model

277 For Ozone And Related Chemical Tracers (MOZART) global simulation

278 (https://acom.ucar.edu/wrf-chem/mozart.shtml). For the inner D2 and D3 domain, ICs

279 and BCs are extracted from the simulation results of the outer domains. Options selected

280 for the CMAQ simulations include the SAPRC07 gas phase chemistry, the AERO7

281 aerosol scheme, the Regional Acid Deposition Model (RADM) model aqueous phase

282 chemistry, ISORROPIA inorganic particulate thermodynamics.

283   The emission inventory developed in this study was used to produce the emission

284 system in the YRD region while emissions beyond YRD were supplied by

285 Multiresolution Emission Inventory for China (MEIC-2017, http://meicmodel.org),

286 Shipping Emission Inventory Model (SEIM) (Liu et al., 2016), and the Model Inter-

287 Comparison Study (MIX) emission inventory for 2010 (Li et al., 2017). The I/SVOC

288 emission inventory outside the YRD region was developed by multiplying the VOCs

289 and POA emissions with the average I/SVOCs-G-to-VOCs and I/SVOCs-P-to-POA

290 ratios of major source categories like industry, vehicle, marine vessel, and residential.

291 Biogenic volatile organic compounds (BVOCs) emissions were estimated based on

292 MEGAN (the Model of Emissions of Gases and Aerosols from Nature) version 2.10

293 driving by inputs of the leaf area index (LAI) from MODIS product, plant functional

294 types (PFT) base on remote sensing data, inline coupled emission factors and

295 meteorology simulated by the WRF model. Detail configurations of MEGAN can be

296 obtained from our previous study (Liu et al., 2018a).
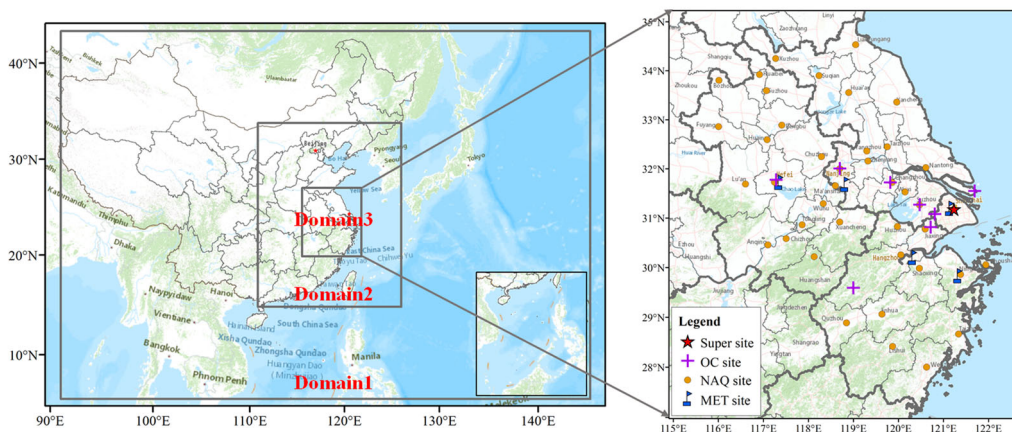
297

298 **Figure 1.** Modeling domain and locations of observation sites. The blue marks are meteorological

299 monitoring sites. The yellow dots represent the national air quality monitoring sites. The purple
300 crosses are the observation sites with PM$_{2.5}$ chemical composition measurements. The red star
301 represents the observation site of AMS measurement.

302   SOA formed from I/SVOCs was estimated using the parameterization within the

303 VBS framework in Lu et al. (2020). Specifically, the I/SVOC surrogates react with OH,

304 generating four oxygenated organic species with volatility spanning from $C^* = 10^{-1}$ to

305 10^2 μg·m^{-3}, which may exist in both gas and condensed phase. The rate coefficient (i.e.,

306 k_{OH}) and product yields (i.e., α_i, i=1, 2, 3, 4) for each primary I/SVOC species were

307 derived based on previous laboratory results (Zhao et al., 2015; Zhao et al., 2016b).

308 Multi-generation oxidation was considered by implementing further oxidation of the

309 vapors from the initial oxidation, which redistributes the mass across the volatility bins

310 of $C^* = 10^{-2}$ to 10^2 μg·m^{-3}, and thus fragmentation and functionalization were included.

311 Additionally, SOA formation from SVOCs were treated similarly, and more details can

312 be found in Murphy et al. (2017). POA was treated as semivolatile to account for its

313 gas-particle partitioning and ageing process and segregated to several particle species,

314 which varied in their volatility that quantified with the metric $C^* = 10^{-1}$ to 10^3 μg·m^{-3}

315 (Donahue et al., 2006). I/SVOCs-P emissions from different sources were then

316 speciated and input as semivolatile accordingly. The remaining POA emissions

317 excluding I/SVOCs-P were treated as nonvolatile POC (primary organic carbon) and

318 PNCOM (primary non-carbon organic matter).

319 2.3 Model simulations

320   To investigate the model performance on OA simulations and the contributions of

321 different sources, we set 14 simulation cases using brute-force method (Zhang et al.,

322 2005). Table 1 shows the settings for these 14 cases. First was BASE simulation case,

323 in which the I/SVOC emissions was not included and the POA emissions were treated

324 as non-volatile. The second was the IMPROVE case, which augmented the high-

325 resolution I/SVOC emission inventory established in this study. In addition, the POA

326 emissions in the IMPROVE simulation were split into both non-volatile and

327 semivolatile parts. The non-volatile emissions were obtained by subtracting the

328 I/SVOCs-P from the total POA. The semivolatile emissions, that was I/SVOCs-P

329 emissions, were treated with variable gas–particle partitioning and multigenerational

330 aging in this simulation case. We then used the difference between IMPROVE and

331 BASE cases to evaluate the OA contributions from I/SVOC emissions. CASE1 to

332 CASE12 respectively excluded the VOC and I/SVOC emissions from different sources.

333 We used the differences between IMPROVE and CASE1−12 to quantify the

334 contribution of each source to OA concentration.

335 **Table 1.** Settings of simulation cases.

Name	Sources with added I/SVOC emissions
BASE	none
IMPROVE	all
CASE1	all except industrial process
CASE2	all except industrial solvent-use
CASE3	all except mobile sources
CASE4	all except residential sources
CASE5	all except biomass burning
CASE6	all except biogenic sources
CASE7	without VOCs and I/SVOC emissions
CASE8	all except gasoline vehicle
CASE9	all except diesel vehicle
CASE10	all except diesel machinery
CASE11	all except marine vessel
CASE12	all except cooking

336

Name	Emission settings	Notes
BASE	with VOC emissions, without I/SVOC emissions	base case
IMPROVE	with both VOC and I/SVOC emissions	to quantify the contributions of VOC and I/SVOC emissions to OA by comparing with BASE case
CASE1	only without industrial process VOC and I/SVOC emissions in the region	to quantify the contributions of VOC and I/SVOC emissions from different source categories to OA by comparing with IMPROVE case
CASE2	only without industrial solvent-use VOC and I/SVOC emissions in the region	
CASE3	only without mobile VOC and I/SVOC emissions in the region	
CASE4	only without residential VOC and I/SVOC emissions in the region	
CASE5	only without biomass burning VOC and I/SVOC emissions in the region	
CASE6	only without biogenic VOC emissions in the region	

CASE7	without VOC and I/SVOC emissions in the region
CASE8	only without gasoline vehicle VOC and I/SVOC emissions in the region
CASE9	only without diesel vehicle VOC and I/SVOC emissions in the region
CASE10	only without diesel machinery VOC and I/SVOC emissions in the region
CASE11	only without marine vessel VOC and I/SVOC emissions in the region
CASE12	only without cooking VOC and I/SVOC emissions in the region

337 2.4 Model evaluation

338   To capture the characteristics of OA with different meteorological features in the

339 YRD region, we selected four periods to represent spring (Mar. 15th to Apr. 15th, 2019),

340 summer (Jul. 1st to 31st, 2019), autumn (Oct. 15th to Nov. 15th, 2018), and winter (Dec.

341 1st to 31st, 2018) to conduct the simulations. Evaluations on model performance were

342 made by comparing the simulation results with the observations obtained in the region,

343 including 5 meteorological observation sites, 10 PM$_{2.5}$ chemical composition sites, and

344 41 national air quality monitoring sites, one in each city. The locations of the

345 meteorological and air pollutant observation sites are shown in Figure 1.

346   We also used the observation data of an AMS and a GC-MS/FID system at the

347 supersite in Shanghai to further verify the model performance on the simulation of POA,

348 SOA, and key VOC precursors. Details of AMS measurements and PMF analysis are

349 provided in our previous study (Huang et al., 2021). A total of 55 PAMS (Photochemical

350 Assessment Monitoring Stations) species were identified by the GC-MS/FID system

351 including 27 alkanes, 11 alkenes, acetylene and 16 aromatics. The supersite was located

352 on the top-floor of an eight-story building in Shanghai Academy of Environmental

353 Sciences (SAES, 31°10' N, 121°25'E), 30 m above the ground. The site was in a typical

354 residential and commercial area with significant influence from traffic emission.

355 Several petrochemical and chemical industrial factories sit around 50 km away from

356 the site to the south and southwest.

357   Model performance in simulation of meteorological parameters and major criteria

358 air pollutants are summarized in Table S5 and S6. The mean bias (MB), mean gross

359 error (MGE), root-mean-square error (RMSE), and index of agreement (IOA) of

360 temperature, humidity, wind speed, and wind direction in each season are within the

361 criteria recommended by Emery et al. (2001). Although the temperature in summer and

362 winter, and wind speed in autumn and winter were slightly overestimated, their MGE

363 and IOA values are within the uncertainties as recommended in Emery et al. (2001).

364 For the simulation of major criteria air pollutants, both mean fractional bias (MFB)

365 and mean fractional error (MFE) of all pollutants met the criteria recommended by

366 Boylan and Russell (2006). Since the addition of I/SVOC emissions would change the

367 $PM_{2.5}$ simulation results, we thus presented the statistical results for both BASE and

368 IMPROVE cases in the Table S6. The modeled SO_2 was slightly overestimated, which

369 is likely due to the faster than expected reduction of SO_2 emissions, resulting in

370 overestimation of SO_2 emissions in the emission inventory. On the contrast, the

371 modeled NO_2 were underestimated in spring, autumn, and winter, likely due to the

372 overestimation of wind speed in these seasons. The modeled O_3 and $PM_{2.5}$ were slightly

373 overestimated in the IMPROVE simulation case. Overall, the simulated meteorological

374 parameters and major criteria air pollutants are consistent with the observations.

375 **3. Results and discussion**

376 3.1 I/SVOC emission inventory

377 3.1.1 Source-specific I/SVOC emissions

378 Table 2 shows the I/SVOCs-G and I/SVOCs-P emission inventoriesI/SVOC

379 emission inventories in gas- and particle-phase for detailed source category for year

380 2017 in the YRD region. The total I/SVOC-G emission in the YRD region was

381 1148.421128.26 Gg in 2017, lower than that in Wu et al. (2021) of 1360 Gg, but higher

382 than the estimate in Huang et al. (2021b) of 730 Gg. The I/SVOC emissions in both Wu

383 et al. (2021) and Huang et al. (2021b) were estimated by the POA scaling factor method.

384 However, I/SVOCs-G emissions usually have stronger correlation with AVOCs, which

385 is fully in gas-phase, other than POA in particle-phase (Lu et al., 2018). Especially for

386 the industrial sectors, where gaseous organics dominate the primary organic emissions,

387 ~~there must be considerable uncertainties if POA scaling factor method is used for the~~

388 ~~estimation of I/SVOCs-G emissions.~~

389   We found industrial solvent-use was the largest contributor (48~~9.38~~3.64 Gg,

390 ~~43.38~~42.11%) of total S/IVOCs-G emissions, followed by industrial process sources

391 (24~~9.3~~4.65 Gg, ~~22~~21.~~10~~30%), mobile source (3~~20~~44.40 ~~-31~~ Gg, ~~28~~29.~~40~~98%),

392 residential source (~~58.57~~62.23 Gg, 5.~~19~~42%), and agriculture source (1~~0.56~~3.58 Gg,

393 ~~0.94~~1.18%). Specifically, chemical production, textile, and solvent-based coating were

394 major sectors of I/SVOCs-G emissions in the YRD region, accounting for 2~~1.59~~0.80%,

395 ~~20.37~~19.51%, and 15.~~33~~07% of the total I/SVOCs-G emission, and their contributions

396 to AVOC emissions were 20.70%, 2.22%, and 23.42%, respectively (See Table S3). It

397 is interesting to note that the I/SVOCs-to-VOCs ratios are largely different for different

398 sources. For example, the textile industry only accounted for 2.22% of the total AVOC

399 emissions in the YRD region but contributed to ~~20.37~~19.51% of the I/SVOC-G

400 emissions due to its higher I/SVOCs-to-VOCs ratio (2.473). Another example is water-

401 based coatings, whose VOC emissions were approximately 10.2% of solvent-based

402 coatings, while their I/SVOC emissions were 29.1% of those from solvent-based

403 coatings. These findings indicate that reductions in VOC emissions not necessarily

404 corresponds to the simultaneous reductions in I/SVOCs emissions and subsequent SOA

405 formation, which should be considered in future control strategies. (Yuan et al., 2010).

406   For I/SVOCs-G emission of mobile origin, the major contributors were gasoline

407 vehicle, diesel vehicle, and non-road diesel machinery, accounting for 13.~~52~~64%,

408 ~~10.59~~11.66%, and ~~3.96~~2.11%, respectively. The total I/SVOCs-G emissions from

409 gasoline and diesel vehicles were 2~~72.03~~90.57 Gg, much higher than the results

410 reported in Liu et al. (2017) (29.58 Gg) and Huang et al. (2021b) (16.0 Gg) using the

411 emission factor method, which likely underestimates the emission factors of I/SVOCs

412 due to the lack of localized emission factors. Our tunnel experiment results show that

413 the average IVOCs emission factors of gasoline and diesel vehicles were 15.3 mg·km^{-}

414 ^{1} and 219.8 mg·km^{-1} (Tang et al., 2021), which were significantly higher than those

415 used in the above studies (Liu et al., 2017; Huang et al., 2021b). More comprehensive

416 localized emission measurements are advocated to better constrain the I/SVOC

417 emissions from mobile sources.

418   I/SVOCs-P emissions were 82.96~~118.39~~ Gg~~, occupying 58.70% of the POA~~

419 ~~emissions in the region. POA emissions and contributions from different sources can~~

420 ~~be found in Table S3.~~ The largest contributor of I/SVOCs-P emissions came from

421 cooking emission~~biomass burning~~ and diesel vehicle, accounting for 53.24%~~58.08%~~

422 and 11.88%~~20.53%~~ of the total, followed by gasoline vehicle (5.23%~~7.12%~~), marine

423 vessel (2.66%), diesel machinery (2.54%), and biomass burning (1.75%~~6.08%~~)~~, diesel~~

424 ~~machinery (4.14%), and marine vessel (4.05%)~~. Note that the I/SVOCs-P emissions

425 from coal combustion (e.g. power plants, boilers, etc.), other industrial processes, and

426 aircraft were not included in this study. On the one hand, the POA emissions (See Table

427 S3) from these sources were limited, accounting for less than 5%, which could be

428 expected that their I/SVOCs-P emissions were also relatively low. On the other hand,

429 the profiles of I/SVOCs-P components of these sources were still difficult to obtain.

430 More measurements of the I/SVOC emissions from these sources is very necessary in

431 the future.

432 **Table 2.** Source-specific emissions of I/SVOCs for the year 2017 in the YRD region.

Source		I/SVOCs		I/SVOCs-G		I/SVOCs-P	
		Gg	%	Gg	%	Gg	%
Industrial process	Oil refinery	5.63	0.46	5.62	0.49	0.01	0.01
	Chemical production	243.60	19.78	238.91	20.80	4.69	5.65
	Pulp and paper	0.11	0.01	0.11	0.01	0.00	0.00
Industrial solvent-use	Textile	229.78	18.66	224.06	19.51	5.72	6.90
	Leather tanning	3.83	0.31	3.83	0.33	0.00	0.00
	Timber processing	31.08	2.52	31.08	2.71	0.00	0.00
	Furniture coating	1.32	0.11	1.32	0.12	0.00	0.00
	Solvent-based coating	173.02	14.05	173.01	15.07	0.00	0.00
	Water-based coating	50.32	4.09	50.32	4.38	0.01	0.01
	Dry cleaning	0.02	0.00	0.02	0.00	0.00	0.00
	Paint remover	0.01	0.00	0.01	0.00	0.00	0.00
Mobile source	Gasoline vehicle	161.01	13.08	156.67	13.64	4.34	5.23

	Diesel vehicle	143.76	11.67	133.90	11.66	9.86	11.88
	Fuel evaporation	0.69	0.06	0.69	0.06	0.00	0.00
	Diesel machinery	49.62	4.03	47.51	4.14	2.11	2.54
	Marine vessel	7.12	0.58	4.91	0.43	2.21	2.66
	Aircraft	0.64	0.05	0.64	0.06	0.00	0.00
Residential source	Coal combustion	2.73	0.22	2.73	0.24	0.00	0.00
	Residential solvent-use	35.29	2.87	35.20	3.07	0.09	0.11
	Cooking	76.77	6.23	24.30	2.12	52.46	63.24
Agriculture source	Biomass burning	15.04	1.22	13.58	1.18	1.45	1.75
	Total	1231.38	100.00	1148.42	100.00	82.96	100.00

433

Source		I/SVOCs-G		I/SVOCs-P	
		Gg	%	Gg	%
Industrial process	Oil refinery	5.63	0.50		
	Chemical production	243.60	21.59		
	Pulp and paper	0.11	0.01		—
Industrial solvent-use	Textile	229.78	20.37	—	
	Leather tanning	3.83	0.34		
	Timber processing	31.08	2.76		
	Furniture coating	1.32	0.12		
	Solvent-based coating	173.02	15.33		
	Water-based coating	50.32	4.46		
	Dry cleaning	0.02	0.00		
	Paint remover	0.01	0.00	—	—
Mobile source	Gasoline vehicle	152.58	13.52	8.44	7.12
	Diesel vehicle	119.45	10.59	24.31	20.53
	Fuel evaporation	0.69	0.06		
	Diesel machinery	44.72	3.96	4.90	4.14
	Marine vessel	2.33	0.21	4.79	4.05
	Aircraft	0.64	0.06		—
Residential source	Coal combustion	2.73	0.24	—	
	Residential solvent-use	35.29	3.13		
	Cooking	20.55	1.82	68.76	58.08
Agriculture source	Biomass burning	10.56	0.94	7.19	6.08
	Total	1128.26	100.00	118.39	100.00

434   3.1.2 Volatility distributions of I/SVOCs

435   Figure 2 shows the volatility distribution of I/SVOC emissions from different

436   sources as well as their gas-particle distributions. The I/SVOC emissions generally

437 showed an increasing trend with the increase of volatility. With the I/SVOC emission

438 profiles of each source category (Table S1 and S2), we successfully compiled the

439 volatility distribution of I/SVOC emissions from different sources as well as their gas-

440 particle distribution (Figure 2). The I/SVOC emissions generally showed an increasing

441 trend with the increase of volatility. As shown in Figure 2(a), IVOC emissions (logC*

442 bins at 3−6) accounted for 8986% of the total I/SVOCs emissions, overwhelmingly

443 dominated by industrial process and mobile sources. SVOCs (logC* bins at 0−2) and

444 low-volatile organic compounds (LVOCs, logC* bins at -1) contributed to 10% and 1%

445 of the total I/SVOCs emissions. In terms of the contributing sectors, mobile sources,

446 industrial process, and solvent-use dominated the total I/SVOC emissions. While the

447 IVOCs were equally contributed by above-listed three sources, industrial process and

448 mobile sources dominated the SVOCs and LVOCs emissions.

449 We further investigated the contributions of different volatility bins to each source

450 category. The mobile source was dominated by IVOC emission (88%). Note that IVOCs

451 in vehicle exhaust are dominated by aromatics, which have faster OH reaction rates and

452 higher SOA yields compared to aliphatics in the same volatility bin (Zhao et al., 2016b;

453 Drozd et al., 2019). Lu et al. (2020) therefore defined two additional lumped IVOC

454 species with logC* bins at 5 and 6 to account for the aromatic IVOCs in vehicle exhaust

455 according to the measurements in previous studies (Zhao et al., 2015; Zhao et al.,

456 2016b). Here in this study, we also split the aromatic IVOC emissions from mobile

457 sources and found that aromatic IVOCs accounted for 23% of the total I/SVOC

458 emissions from the mobile source. Note that we also split the aromatic IVOCs emission

459 from mobile source using the method in Lu et al. (2020) and found that aromatic IVOCs

460 accounted for 23% of the total I/SVOC emissions from the mobile source. The

461 industrial process and solvent-use sources were also dominated by IVOC emissions,

462 accounting for 81% and 97%, respectively. The volatility distribution of residential

463 sources was relatively uniform, with IVOCs, SVOCs and LVOCs accounting for 4640%,

464 2730%, and 2730%. Agricultural (i.e., biomass burning) sources were more

465   concentrated in IVOCs, accounting for ~~71~~76%, while SVOCs ~~and LVOCs~~ accounted

466   for 2~~0% and 94~~%, respectively. ~~Except agricultural sources, I/SVOC emissions from~~

467   ~~all sources are dominated by gas-phase species. The agricultural sources were~~

468   ~~dominated by particle-phase species, taking up 78% of the total I/SVOC emissions with~~

469   ~~the VBS bins concentrated in the logC* range of 0~4.~~ It should be noted that other than

470   mobile sources, the emission profiles of the other sources were mainly derived from

471   SPECIATE 5.1 database (US EPA, 2021) in this study, which may be inconsistent with

472   real-world emissions in China. To further reduce the uncertainty in this newly establish

473   I/SVOC estimation inventory, measurements of I/SVOC emissions from different local

474   sources are therefore important and urgently needed in the future.
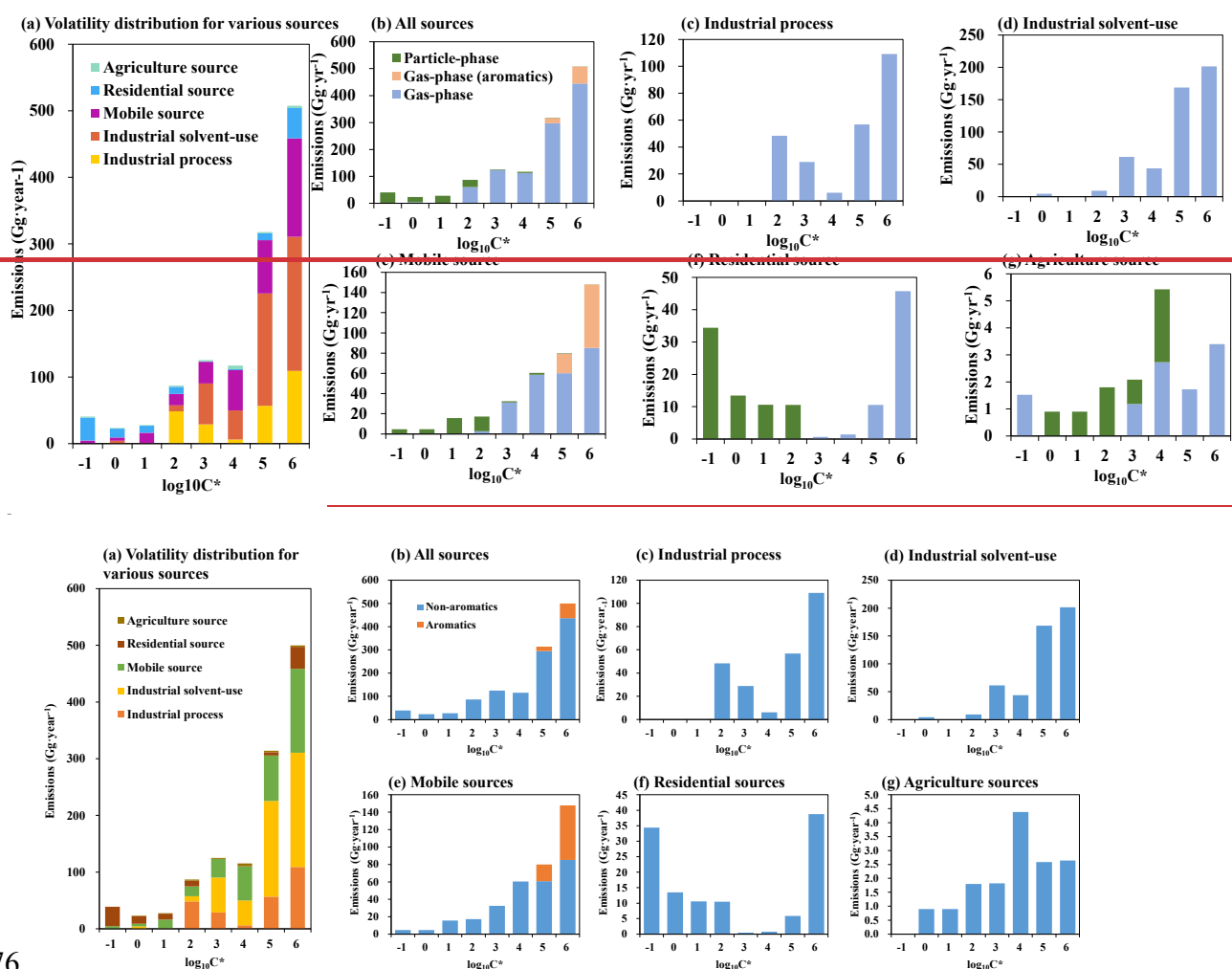
477   **Figure 2.** Volatility distributions of I/SVOCs emitted from different sources in the YRD region.

478 3.1.3 Spatial distributions of I/SVOC emissions in YRD region

479   Figure 3 compares the spatial distributions of AVOC, IVOC, SVOC, and LVOC

480 emissions in the YRD region. The IVOC, SVOC, and LVOC emissions were largely

481 concentrated in city clusters in eastern YRD, and hotspots can also be observed in the

482 northern agglomerations. The distributions of I/S/LVOC emissions were generally

483 consistent with that of the AVOC emissions in the region. Compared to the spatial

484 distributions of I/S/LVOC emissions in Chang et al. (2022), our emissions had similar

485 spatial distributions but at a higher resolution. Emission hotspots in urban areas can be

486 captured more clearly in this study, which will help improve the simulation in urban

487 areas.

488   Figure ~~3~~ 4 shows the spatial distributions of source-specific I/SVOC emissions in

489 the YRD region. There were considerable differences in the spatial distributions of

490 I/SVOC emissions from different sources. The I/SVOC emissions from industrial

491 sources (including industrial process and industrial solvent-use) were mainly

492 concentrated in the eastern urban agglomeration, which was related to the developed

493 industrial activities in the region. ~~The I/SVOC emissions were largely concentrated in~~

494 ~~city clusters in eastern YRD, and hotspots can also be observed in the northern urban~~

495 ~~agglomerations. The spatial distribution of total I/SVOC emissions was resulted from~~

496 ~~combined emissions from mobile, industrial process and solvent-use sources.~~ The

497 I/SVOC emissions from mobile and residential sources clustered into multiple hotspots

498 in urban areas, while emissions from agricultural sources were mainly distributed in

499 northern YRD, where frequent agricultural activities exist. ~~The distribution of I/SVOC~~

500 ~~emissions was generally consistent with that of the VOC emissions in the eastern and~~

501 ~~central area of the region. But higher I/SVOC emissions than VOC emissions were~~

502 ~~observed in northern YRD (See Figure S1). This can be explained by the difference in~~

503 ~~I/SVOCs-G-to-VOCs ratios among different sources. For example, industrial and~~

504 ~~mobile sectors are major sources of I/SVOC emissions, yet AVOC emissions were~~

505 ~~mainly dominated by industrial sectors.~~

506   We also compare the spatial distributions of I/SVOC emissions with those of POA

507   and BVOCs. We found that POA emissions were more concentrated in urban centers

508   associated with mobile and residential sources (See Figure S1). BVOC emissions in the

509   YRD region were mainly distributed in the southern area, where AVOC and IVOC

510   emissions were relatively low. The difference in the spatial distributions of I/SVOC,

511   AVOC, BVOC, and POA emissions implies that the sources of organic components in

512   different areas of the region are quite different, which will be discussed in the following

513   sections.
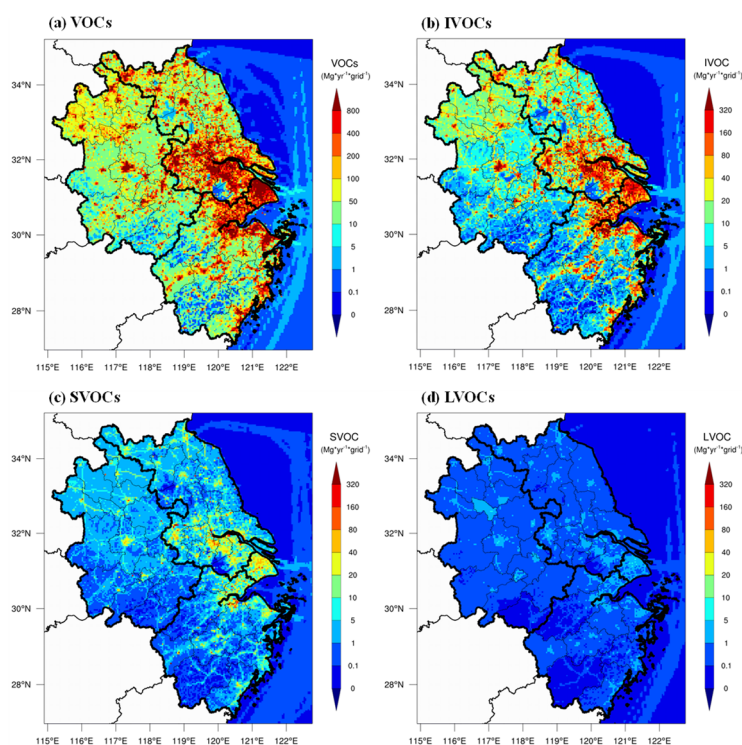
514

515   **Figure 3.** Spatial distributions of anthropogenic VOC, IVOC, SVOC, and LVOC emissions in the
516   YRD region for the year 2017.
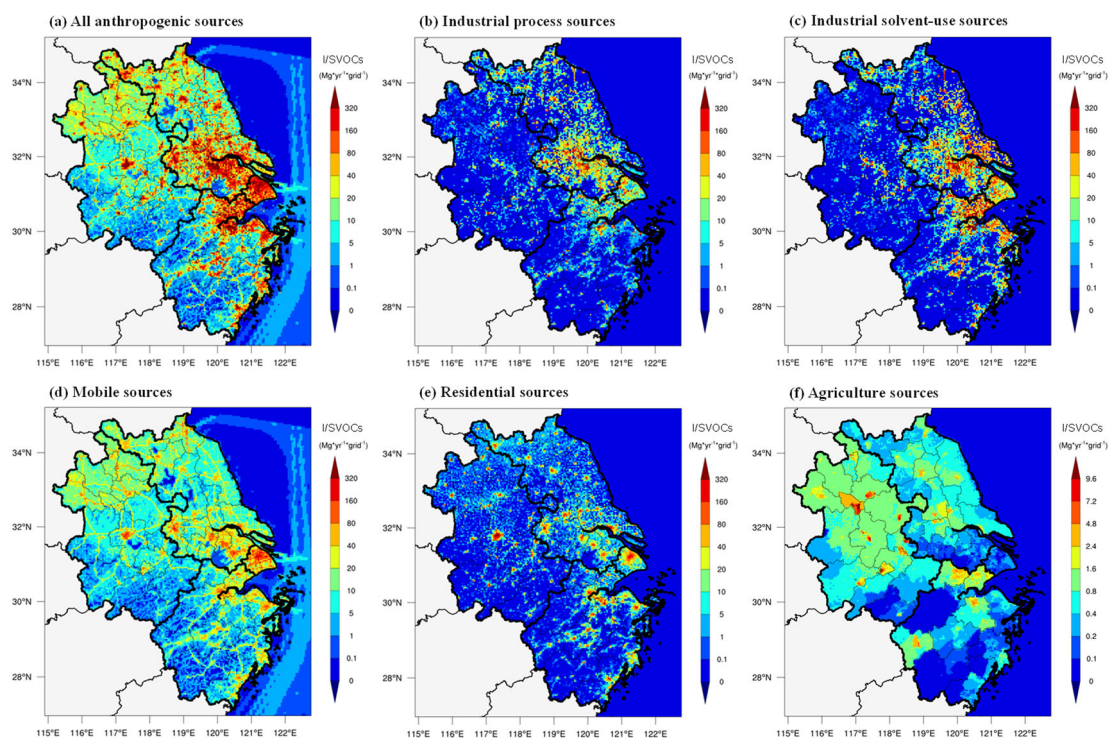
517

518 **Figure 3~~4~~**. Spatial distributions of I/SVOC emissions from different source categories in the YRD

519 region for the year 2017.

520 3.2 Comparison between model simulation and observation

521 3.2.1 Simulation results of VOCs and IVOCs

522 Since model performance on the simulation of VOCs are critical for SOA

523 estimation, we first compare the modeled concentrations of VOCs with those of the

524 measured at the SAES supersite for several aromatic VOCs, including benzene, toluene,

525 and m-/p-/o-xylenes. As shown in Figure S2, the model simulation was able to capture

526 the hourly variations of these species measured, with Pearson correlation coefficients

527 (r) of 0.54−0.65, 0.45−0.60, 0.54−0.69 for toluene, xylene, and benzene respectively.

528 Although the simulation results of toluene were 28% lower and xylene and benzene

529 were 41% and 22% higher than those of the measured, the model results are within the

530 uncertainties. Overall, the simulation results of the VOC species showed good

531 agreements with the observations, which could be further used for the model simulation

532 of SOA formation.

533 Long-term continuous observations of I/SVOC concentrations were sparse, so the

534 simulation results of IVOCs were compared with those obtained from offline

535 measurements reported in our previous studies (Li et al., 2019; Ren et al., 2020). The

536 reported IVOC concentrations (sum of gas- and particle-phase concentrations) in

537 summer and winter Shanghai in 2018 respectively varied between 1.5−17.2 and

538 2.2−43.1 µg·m^{-3} with average concentrations of 6.8 ± 3.7 and 18.2 ± 11.0 µg·m^3. In this

539 study, our modeled average concentrations of IVOCs in spring, summer, autumn, and

540 winter at the SAES supersite in Shanghai were 12.8 ± 5.6, 9.0 ± 3.2, 12.2 ± 5.2, and

541 12.4 ± 7.6 µg·m^{-3}, respectively. Although there was still a deviation of 20%−30%

542 between the simulation and observation, not to mention the diurnal patterns and spatial

543 distributions also remained unknown, the simulation results are at least comparable to

544 those of the measured concentrations, suggesting the modeled I/SVOCs is appropriate

545 to be used in the estimation of SOA production from different sources. Continuous long-

546 term measurements of I/SVOC at multiple locations are strongly recommended in the

547 future to improve the model performance and reduce the uncertainties in SOA

548 estimation.

549 3.2.1 Simulation results of OA concentrations

550   Figure 4 5 presents the OA concentrations originated from different sources,

551 including POA and SOA formed from AVOCs, BVOCs, and I/SVOCs, in four seasons

552 in YRD from both BASE and IMPROVE simulations. Here we used the average of the

553 modeled concentrations at 41 national air quality monitoring sites (See the yellow dots

554 in Figure 1) to represent the regional average. The regional average concentration of

555 OA (9.62 8.75 µg·m^{-3}) in the IMPROVE simulation was 38 22% higher than that from

556 BASE simulation (6.98 7.17 µg·m^{-3}) due to the involvement of I/SVOCs in the

557 IMPROVE simulation.

558   The seasonal average concentration of POA was 5.0 5 µg·m^{-3} in the BASE case,

559 with the lowest in summer (3.3 8 µg m^{-3}) and the highest in winter (5 6.9 µg m^{-3}). High

560 POA concentrations in winter was mainly induced by the stagnant meteorological

561 conditions such as low wind speed and boundary layer height, and vice versa in summer.

562 For the spatial distributions as presented in Figure 5 6, POA concentrations in northern

563 YRD were high and mainly concentrated in urban areas, which was consistent with the

564 distributions of POA emissions (Figure S1). The POA concentrations in the IMPROVE

565 simulation decreased by 12%−20% compared with the BASE case. ~~The POA~~

566 ~~concentrations in the IMPROVE simulation were -3%−13% apart from those in the~~

567 ~~BASE simulation.~~ In the IMPROVE simulation, the POA was treated as semi-volatile,

568 where gas–particle partitioning and multigeneration oxidation were considered

569 (Murphy et al., 2017). Entering into the atmosphere, more semi-volatile compounds

570 evaporated into gas-phase and then generated SOA through multigeneration oxidation,

571 which reduced the POA concentrations relatively. ~~The differences between these two~~

572 ~~cases were then determined by the competitive effects of functionalization and~~

573 ~~fragmentation. In summer, more aged products were transferred to higher-volatility bins~~

574 ~~to produce SOA and thus reduced POA concentrations.~~

575 ~~BASE and IMPROVE simulations show similar results in the average~~

576 ~~concentrations of SOA formed from AVOCs (AVSOA).~~ The seasonal average

577 concentration of AVSOA was only 0.~~25~~22 μg·m^{-3}. The average AVSOA concentration

578 in the IMPROVE case increased by 17% compared with the BASE case due to higher

579 OA loading. Nonetheless, AVSOA still~~,~~ ~~exhibiting~~ exhibited very limited contribution

580 to the regional OA concentration, whereas average concentration of BVOC derived

581 SOA (BVSOA, 1.7 μg m^{-3} in the IMPROVE simulation case) was much higher than

582 expected. Also, evident seasonal variations were observed for BVSOA, with the highest

583 in summer (~~2.48~~2.27 μg·m^{-3}), followed by spring (1.~~80~~65 μg·m^{-3}), autumn (1.~~36~~62

584 μg·m^{-3}), and winter (1.~~19~~11 μg·m^{-3}). Hotspots of BVSOA concentrations were

585 concentrated in the western and southern YRD. The observed seasonal variations and

586 spatial distributions of BVOC derived SOA were consistent with those of the BVOC

587 emissions in YRD (Liu et al., 2018a).

588 The average concentration of I/SVOC derived SOA (I/SVSOA) in IMPROVE

589 simulation was 2.~~26~~18 μg·m^{-3}, with the highest in spring (2.~~73~~66 μg·m^{-3}) and the

590 lowest in summer (1.~~87~~79 μg·m^{-3}), which is a combined effect of emission, oxidation

591   and meteorological conditions. For example, Qin et al. (2022) suggested that in spring

592   the enhanced solar radiation and OH oxidation potentially promote the secondary

593   conversion from I/SVOCs to SOA. The low concentration in summer was likely due to

594   the better meteorological conditions than the other seasons. By incorporating I/SVOC

595   emissions into the IMPROVE simulation, the modeled average SOA concentration in

596   the region increased from 1.~~96~~ 66 (BASE) to 4.~~22~~ 10 μg·m^{-3}; and high concentrations

597   of I/SVSOA were observed in central and northern YRD. Overall, the addition of high-

598   resolution I/SVOC emissions significantly increase the SOA concentration by ~~116~~148%,

599   which will be further constrained by the observation in next section.

600   To validate the model performance on regional OA simulation, we compared it

601   with the measured concentrations of organic carbon (OC) in PM$_{2.5}$ at multiple sites in

602   the YRD region (Figure S3). Although both BASE and IMPROVE simulations showed

603   good correlations with the observation as shown in Figures S3c, S3f, S3i, and S3l~~6c, 6f,~~

604   ~~6i, and 6l~~, OC concentrations in IMPROVE simulations in different seasons were all

605   higher than those in the BASE simulations. In the BASE simulation, the modeled OC

606   concentrations of each season only explained ~~49~~51% to ~~59~~71% of the observations.

607   With the addition of I/SVOC emissions into IMPROVE simulation, the modeled OC

608   concentrations much better agreed with the observations, with modeled OC increased

609   to ~~75~~70% to ~~93~~91% of the observations. Details for the statistical evaluation of model

610   performance on OC in BASE and IMPROVE simulations are shown in Table ~~S6~~S7.
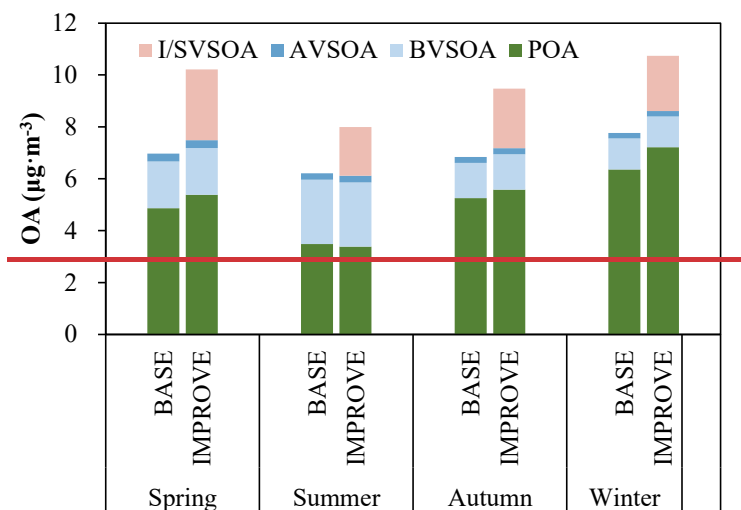
611
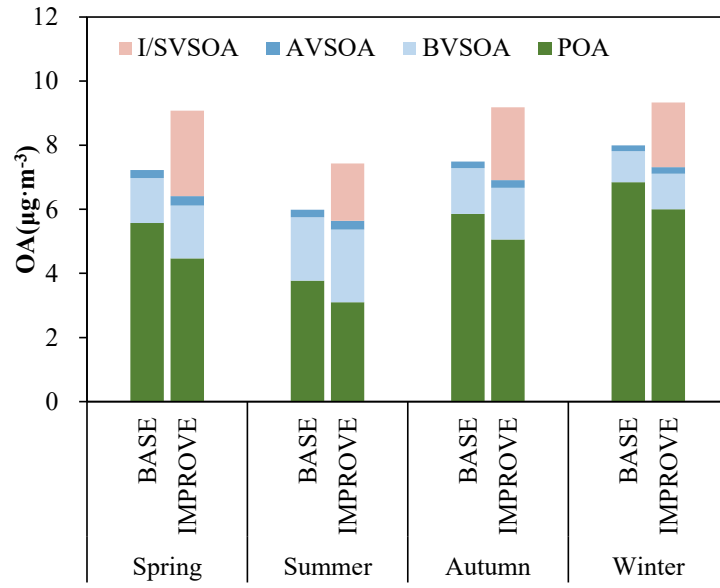
612

613 **Figure 45.** Comparisons of the regional average concentrations of POA and SOA formed from

614 AVOCs, BVOCs, and I/SVOCs in different seasons from the BASE and IMPROVE simulations.

615
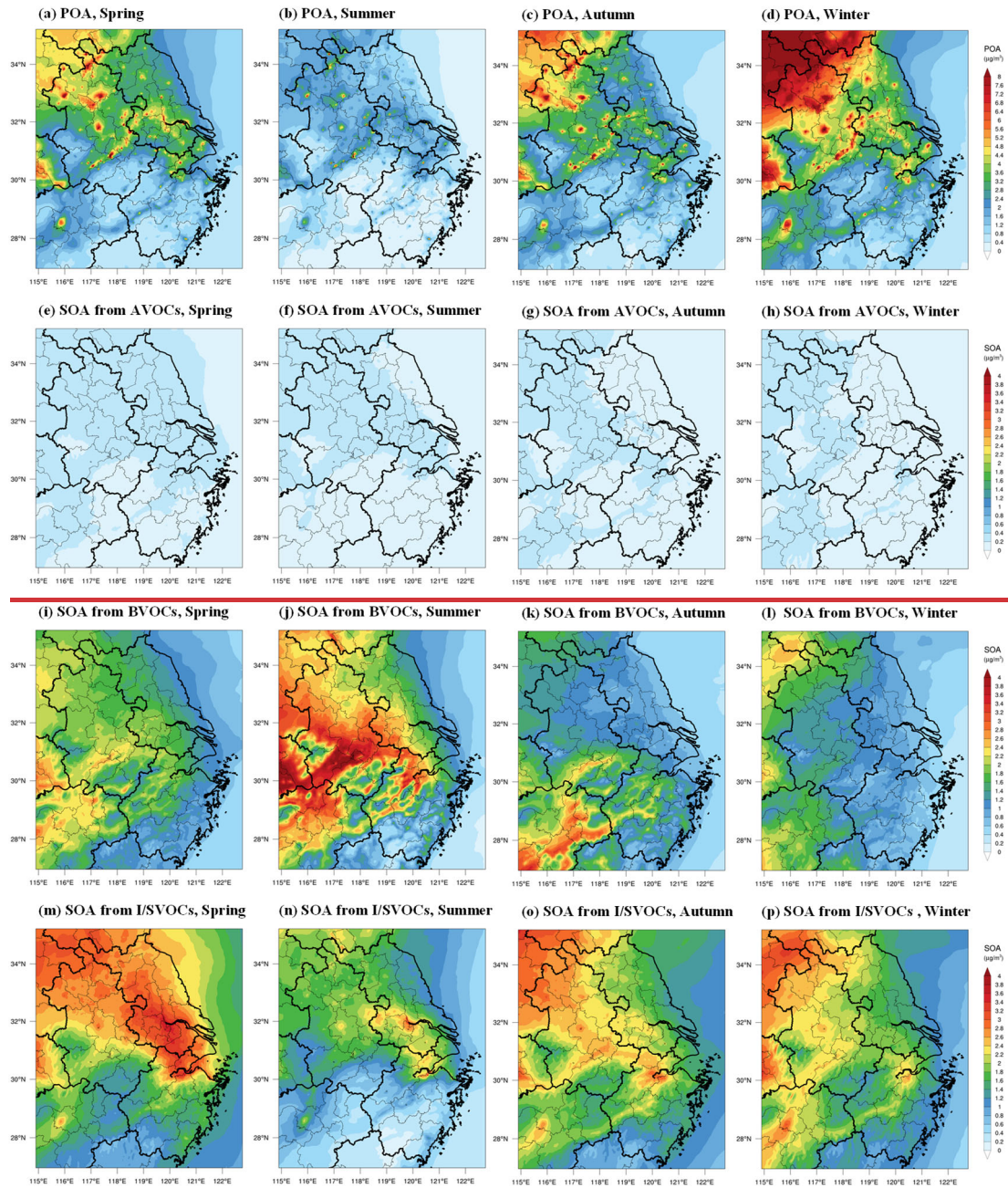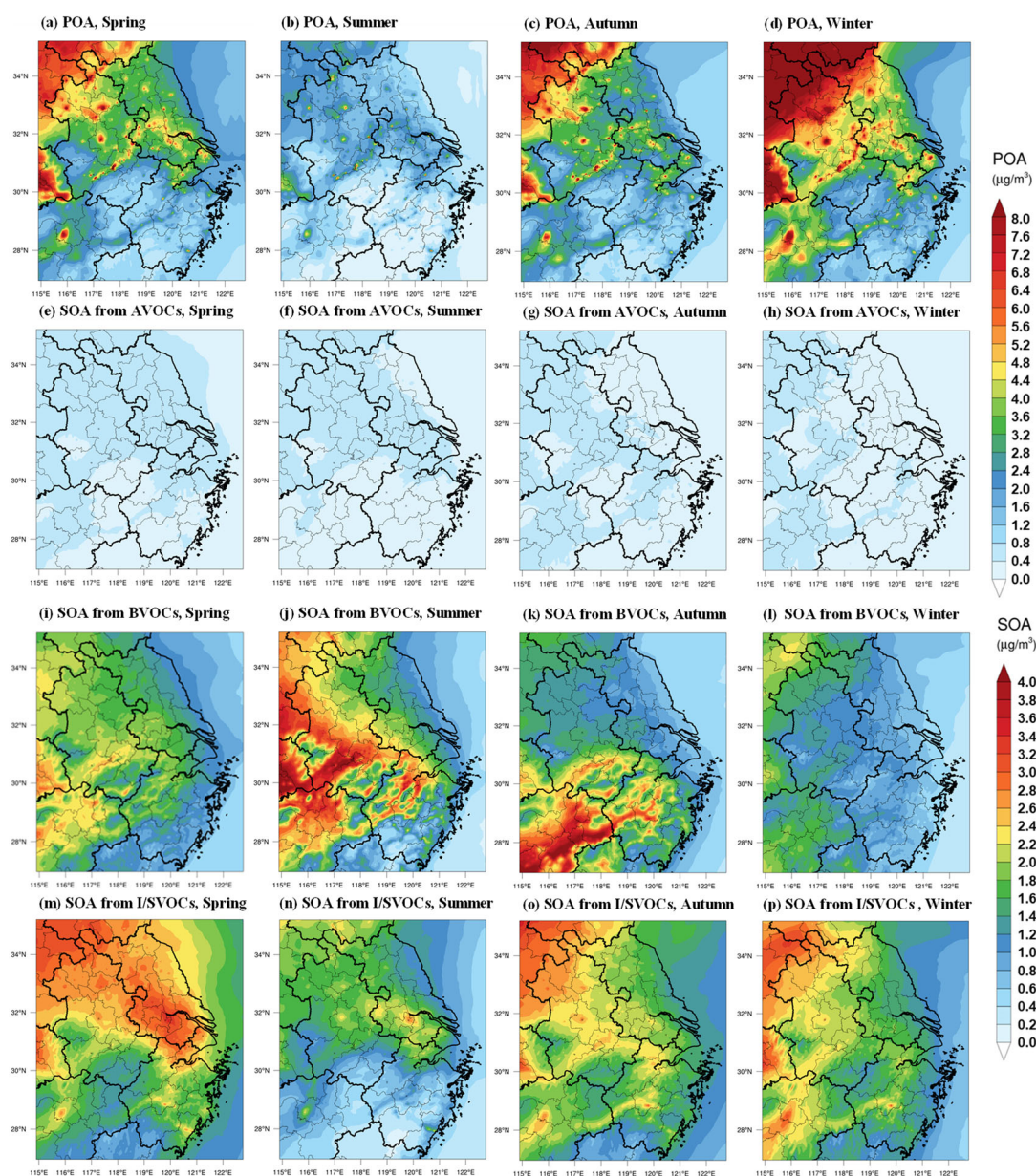
616

617 **Figure 5̶6.** Spatial distributions of modeled POA and SOA formed from AVOCs, BVOCs, and
618 I/SVOCs in different seasons in the IMPROVE simulation.

619 3.2.2 Temporal variations of OA components: simulation vs. AMS observation

620   To further validate the model performance on the simulations of POA and SOA,

621 we compared the simulation results with those measured by an AMS at the SAES

622 supersite. Both simulation and observation results were obtained for PM_1 aerosol

623 particles (aerodynamic diameter < 1 µm). Figure 6̶7 shows that the simulation results

624 of POA, SOA and OA were similar to the observation results not only in average

625 concentration levels but also in temporal variations. For POA, the BASE and

IMPROVE simulations agree with each other (Figure S4) and both can reproduce the observed concentrations and diurnal variations of POA though a small deviation of ~~3~~4%−~~26~~18% between the simulated and observed concentrations in different seasons still existed. Similar to the observation results, the simulated POA concentrations peaked at noon and early evening, which were mainly contributed by cooking emissions as reported in our previous study (Huang et al., 2021).

For SOA, the average concentrations in spring, summer, autumn, and winter in BASE simulation were 1.~~4~~2, 1.6, 0.8, and 0.7 μg·m^{-3}, respectively, which were only ~~13~~14%−~~31~~30% of those observed by the AMS (see Figure S4). The SOA simulation was greatly improved in IMPROVE simulation with the modeled SOA concentrations of ~~4.2~~3.8, 3.~~8~~7, 2.7, and 2.~~4~~3 μg·m^{-3} in spring, summer, autumn, and winter respectively. The SOA concentrations in IMPROVE simulation were ~~1~~2.4−~~2~~3.~~4~~6 times higher than those in BASE simulation, which is ~~43~~40% to ~~75~~72% of the observation, indicating the large contributions of I/SVOCs emissions to SOA production.

The IMPROVE simulation also demonstrated improvements in reproducing the temporal variations of SOA, especially during the daytime (Figure ~~6e~~7e - ~~6h~~7h). Compared with the BASE simulation, evident increases in SOA concentrations during daytime can be observed in IMPROVE simulation, which agrees better with the observation, likely driven by photochemistry. Although the SOA simulations were improved in all four seasons, best simulation results were found in summer, when both the concentrations and diurnal variations of SOA were well reproduced.

While our current results presented great improvements in SOA simulation, gaps were still left between the simulation and observation especially during the nighttime. The main reasons for the discrepancy between the simulated and measured SOA are: (1) I/SVOC emissions from outside of the YRD region might be underestimated due to the lack of detailed base emission inventory, resulting in the corresponding underestimation~~s~~ of the transported SOA, which were prominent especially in autumn, winter and spring in Shanghai; (2) current model simulation only consider the oxidation

processes driven by OH oxidation. However, an increasing body of experimental and observational evidence suggest that heterogeneous and multiphase reactions also played important roles in SOA formation especially during pollution episodes (Guo et al., 2020; Kim et al., 2021). Recent studies also found that nocturnal NO_3 oxidation was also an important route for SOA formation (Yu et al., 2019; Decker et al., 2021). Yet mechanism and parameterizations of these processes remain unclear, making the involvement of these processes in the model difficult.
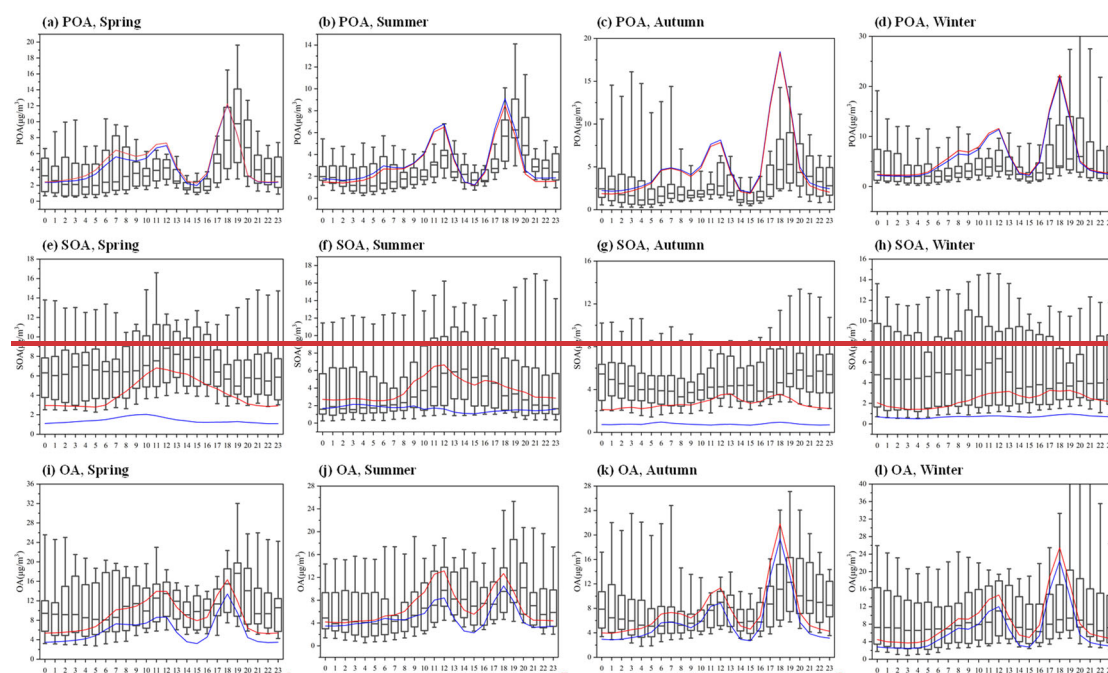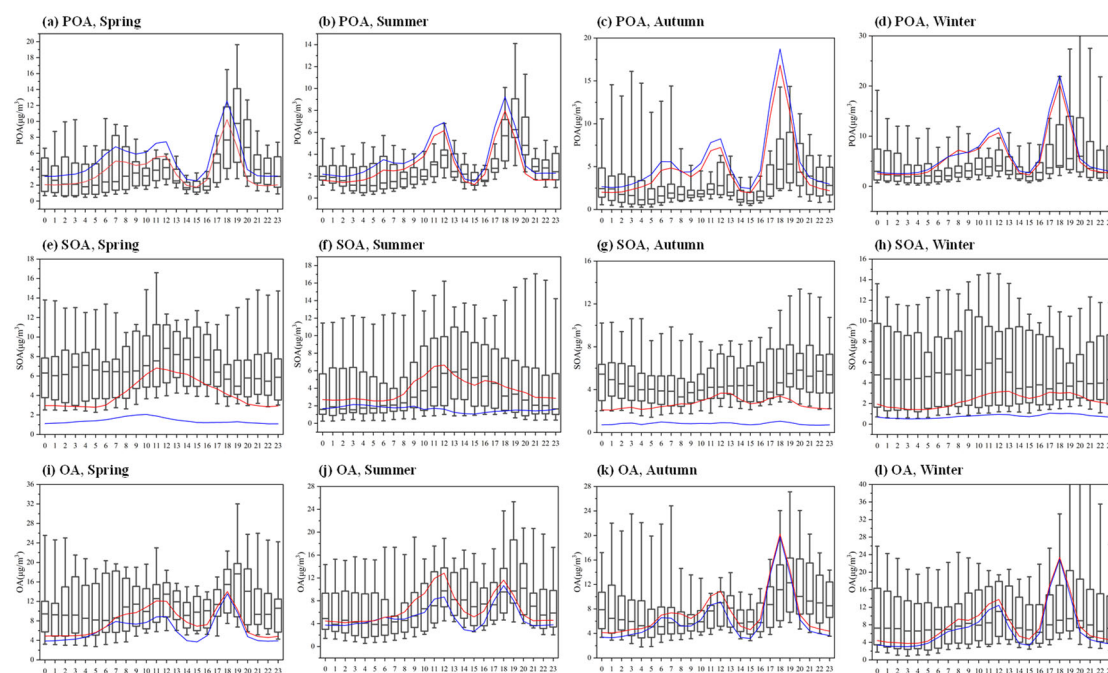
Figure ~~6~~7. Diurnal patterns of modeled POA, SOA, and OA concentrations in different seasons and their comparisons with the observations at the SAES supersite. The boxplots represent the diurnal patterns of the AMS observations. The blue and red lines respectively represent the diurnal patterns of the simulation results in BASE and IMPROVE cases.

3.3 OA source contributions

3.3.1 POA and SOA sources in the region

Based on the high-resolution I/SVOC emission inventory established in this study, we successfully simulated the POA and SOA concentrations from each source. Table 3 summarizes the regional average concentrations of POA and SOA originated from different sources and their relative contributions. Residential POA dominated the regional OA, with average concentrations ranged from 1.~~90~~56 to ~~3.51~~2.35 μg·m^{-3} in different seasons, accounting for ~~23.79~~19.47%−~~32.66~~25.31% of the total OA, among which cooking emission is the dominant source (*ca.* ~~94~~98%) of residential POA. Other POA sources include industrial, biomass burning, and mobile sources, accounting for 8.02%−8.63%, 4.45%−8.28%, and 5.03%−5.78%~~7.25%−8.67%, 4.94%−10.23%, and 3.42%−4.35%~~ of the total OA, respectively. The cumulative fraction of POA in total OA from industrial and mobile sources was 13.44%−14.41%~~10.67%−12.86%~~, close to that of HOA (15%) observed by the AMS measurement in Shanghai (Figure S5).

Industrial sources were the main source of SOA in the YRD region, with average SOA concentrations of 0.84−1.21~~0.91−1.38~~ μg·m^{-3} in four seasons, accounting for 8.98%−15.64%~~8.71%−13.65%~~ of the total OA, among which, industrial process and solvent-use sources had almost equal contributions. Mobile sources were the second largest source of SOA in this region, with an average concentration of 0.31−0.50~~0.37−0.57~~ μg·m^{-3}, accounting for 3.36%−6.69%~~3.42%−6.09%~~ of the total OA. Among them, the source contribution of gasoline vehicles to SOA was 1.77%−3.07%~~1.80%−2.84%~~, and that of diesel vehicles was 1.18%−2.55%~~1.20%−2.44%~~. BVSOA showed significant seasonal differences with concentrations of 0.88, 1.26, 0.70, and 0.11~~0.76, 1.61, 0.59, and 0.12~~ μg·m^{-3}, respectively in spring, summer, autumn, and winter, accounting for 9.64%, 16.94%,

692   7.60%, and 1.15%7.40%, 20.20%, 6.21%, and 1.14% of the total OA.

693   Overall, cooking emission was the major source of POA in YRD, accounting for

694   19.14%−24.99%27.69%−32.45% of the total OA, which is consistent with our

695   observations in Shanghai (Huang et al., 2021; Zhu et al., 2021). Both simulations and

696   observations demonstrated higher contributions of cooking emission in urban China

697   than those reported overseas (17%–18%) (Chen et al., 2021), which is attributed to the

698   difference between Asian-style and Western-style cooking. The results emphasize that

699   cooking emission has become a non-negligible source of non-fossil carbon in urban

700   areas in eastern China. Contributions from industrial sources were running the second

701   among all sources, accounting for 17.02%−24.12%16.51%−21.64% of OA and 24.7%−

702   26.8%23.33%−28.57% of SOA, which is attributed to the high I/SVOC emissions from

703   industrial sources and is consistent with previous studies (Miao et al., 2021). Other

704   sources mainly include mobile sources (8.76% to 11.72%7.77% to 9.68% of OA) and

705   biomass burning (5.19%−8.87%5.63%−11.15% of OA). Specifically, diesel and

706   gasoline vehicles were the major contributors among mobile sources, with higher

707   contribution from the former (3.95%−4.66%3.98%−4.68%) than the latter

708   (3.05%−4.02%2.79%−3.73%), followed by diesel machinery

709   (1.32%−2.11%0.86%−1.06%) and marine vessels (0.43%−0.93%0.15%−0.30%). The

710   contribution of biomass burning was highest in winter (8.87%11.15%) compared to

711   contributions of 5.19%−7.28%5.63%−7.29% in other seasons and it was even higher

712   than contribution of mobile sources (8.76%7.77%) in winter. The remaining

713   14.54%−35.64%15.44%−27.03% of OA was from super region scale, which

714   represented OA originated from emissions outside the YRD region. Our results were

715   generally similar with those of Chang et al. (2022) for the YRD region. We both found

716   the domestic combustion mainly engaged in cooking emissions had a major

717   contribution to OA. Next was volatile chemical products (VCPs), especially the use of

718   solvents, paints, and adhesives in industrial sector, also made a high contribution. Note

719   that industrial process also took up a high fraction in our OA simulation, while it was

lower in Chang et al. (2022)'s study. The difference in I/SVOC emission estimates was the main reason for this divergence. Mobile sources in both studies had similar contributions, which accounted for about 10% to total OA. Comparatively, our source classification was more specific, which will help identify more specific OA sources to design more refined regional control countermeasures.

Table 3. POA and SOA source contributions of different emission sources in each season in the YRD region.

Sources	Spring conc. (µg·m⁻³)	Spring ratio (%)	Summer conc. (µg·m⁻³)	Summer ratio (%)	Autumn conc. (µg·m⁻³)	Autumn ratio (%)	Winter conc. (µg·m⁻³)	Winter ratio (%)
POA	4.47	49.19	3.09	41.65	5.05	55.06	6.00	64.29
Industrial sources	0.73	8.02	0.63	8.48	0.79	8.63	0.75	8.04
Industrial process	0.61	6.71	0.54	7.27	0.67	7.29	0.63	6.77
Industrial solvent-use	0.12	1.31	0.09	1.20	0.12	1.34	0.12	1.27
Mobile sources	0.49	5.43	0.37	5.03	0.53	5.78	0.50	5.40
Gasoline Vehicles	0.09	1.01	0.07	0.96	0.12	1.32	0.12	1.28
Diesel Vehicles	0.23	2.58	0.16	2.16	0.26	2.79	0.26	2.77
Diesel machinery	0.10	1.06	0.09	1.21	0.10	1.08	0.09	0.95
Marine vessel	0.07	0.78	0.05	0.70	0.05	0.59	0.04	0.39
Residential sources	1.77	19.47	1.56	20.95	2.32	25.31	2.35	25.16
Cooking	1.74	19.14	1.54	20.72	2.29	24.99	2.31	24.77
Other residential	0.03	0.33	0.02	0.23	0.03	0.33	0.04	0.39
Biomass burning	0.60	6.65	0.33	4.45	0.60	6.58	0.77	8.28
Super region	0.87	9.63	0.20	2.75	0.80	8.75	1.62	17.41
SOA	4.61	50.81	4.34	58.35	4.13	44.94	3.33	35.71
Industrial sources	1.21	13.38	1.16	15.64	1.02	11.10	0.84	8.98
Industrial process	0.68	7.53	0.62	8.39	0.61	6.62	0.53	5.64
Industrial solvent-use	0.53	5.84	0.54	7.25	0.41	4.48	0.31	3.34
Mobile sources	0.49	5.45	0.50	6.69	0.43	4.63	0.31	3.36
Gasoline Vehicles	0.25	2.71	0.23	3.07	0.21	2.25	0.16	1.77
Diesel Vehicles	0.18	1.95	0.19	2.50	0.16	1.73	0.11	1.18
Diesel machinery	0.06	0.66	0.07	0.90	0.05	0.56	0.03	0.37
Marine vessel	0.01	0.13	0.02	0.22	0.01	0.09	0.00	0.04
Residential sources	0.42	4.68	0.49	6.54	0.43	4.71	0.32	3.39
Cooking	0.21	2.34	0.29	3.97	0.26	2.78	0.16	1.71
Other residential	0.21	2.34	0.19	2.58	0.18	1.93	0.16	1.68
Biomass burning	0.06	0.63	0.06	0.74	0.05	0.59	0.06	0.60
Biogenic	0.88	9.64	1.26	16.94	0.70	7.60	0.11	1.15

Sources	Spring		Summer		Autumn		Winter	
	conc. (μg·m⁻³)	ratio (%)	conc. (μg·m⁻³)	ratio (%)	conc. (μg·m⁻³)	ratio (%)	conc. (μg·m⁻³)	ratio (%)
Super region	1.55	17.04	0.88	11.80	1.50	16.30	1.70	18.23

727

Sources	Spring		Summer		Autumn		Winter	
	conc. ($\mu g \cdot m^{-3}$)	ratio (%)	conc. ($\mu g \cdot m^{-3}$)	ratio (%)	conc. ($\mu g \cdot m^{-3}$)	ratio (%)	conc. ($\mu g \cdot m^{-3}$)	ratio (%)
POA	5.38	52.71	3.39	42.40	5.59	58.86	7.21	67.11
Industrial sources	0.83	8.10	0.58	7.25	0.82	8.67	0.84	7.80
Industrial process	0.73	7.19	0.52	6.54	0.73	7.74	0.75	6.98
Industrial solvent-use	0.09	0.91	0.06	0.71	0.09	0.93	0.09	0.82
Mobile sources	0.42	4.11	0.27	3.42	0.40	4.19	0.47	4.35
Gasoline Vehicles	0.10	0.99	0.07	0.89	0.09	0.99	0.11	0.99
Diesel Vehicles	0.26	2.53	0.16	2.01	0.25	2.61	0.30	2.78
Diesel machinery	0.04	0.42	0.03	0.40	0.04	0.45	0.05	0.48
Marine vessel	0.02	0.17	0.01	0.13	0.01	0.14	0.01	0.10
Residential sources	2.63	25.75	1.90	23.79	2.93	30.88	3.51	32.66
Cooking	2.44	23.92	1.85	23.15	2.80	29.54	3.18	29.61
Other residential	0.19	1.82	0.05	0.64	0.13	1.34	0.33	3.05
Biomass burning	0.70	6.88	0.39	4.94	0.56	5.90	1.10	10.23
Super region	0.80	7.88	0.24	3.00	0.87	9.22	1.30	12.07
SOA	4.83	47.29	4.60	57.60	3.90	41.14	3.53	32.89
Industrial sources	1.38	13.54	1.09	13.65	0.91	9.56	0.94	8.71
Industrial process	0.71	6.94	0.53	6.58	0.51	5.38	0.54	4.99
Industrial solvent-use	0.67	6.61	0.57	7.08	0.40	4.18	0.40	3.71
Mobile sources	0.57	5.57	0.49	6.09	0.38	3.98	0.37	3.42
Gasoline Vehicles	0.28	2.70	0.23	2.84	0.18	1.88	0.19	1.80
Diesel Vehicles	0.22	2.15	0.20	2.44	0.15	1.56	0.13	1.20
Diesel machinery	0.06	0.59	0.05	0.66	0.04	0.45	0.04	0.38
Marine vessel	0.01	0.13	0.01	0.14	0.01	0.09	0.01	0.05
Residential sources	0.39	3.78	0.36	4.54	0.26	2.78	0.31	2.84
Cooking	0.39	3.78	0.36	4.54	0.26	2.78	0.31	2.84
Other residential	0.00	0.00	0.00	0.00	0.00	0.00	0.00	0.00
Biomass burning	0.04	0.41	0.06	0.69	0.01	0.11	0.10	0.92
Biogenic	0.76	7.40	1.61	20.20	0.59	6.21	0.12	1.14
Super region	1.69	16.59	0.99	12.44	1.76	18.51	1.70	15.86

728 3.3.2 Spatial distributions of SOA originated from different sources

729 Figure 7 8 shows the spatial distributions of modeled SOA originated from

730 different sources in each season in YRD region. Note that we only considered the SOA

731 formed from the intraregional VOC and I/SVOC emissions, excluding those transported

732 from the super region. A large spatial variability was observed for the sources of SOA

733 driven by emissions. For example, industrial and mobile SOA concentrated in the

734 eastern and central YRD, where I/SVOC emissions were high (Figure 3̶4). Residential

735 and agricultural SOA presented a more uniform spatial distribution than industrial and

736 mobile SOA, with enhanced formation in central and western YRD (Figures 7̶i̶8i-7̶l̶8l).

737   Although absolute source-dependent SOA concentrations differ in different

738 seasons, low spatial variabilities were observed for different seasons. Industrial, mobile,

739 and residential sources were the predominant contributors to SOA formation in eastern

740 and central YRD, especially for the area along the Hangzhou Bay and Yangtze River

741 driven by the enhanced I/SVOC emissions. The spatial distributions of BVSOA have

742 been discussed above and will not be detailed here.

743
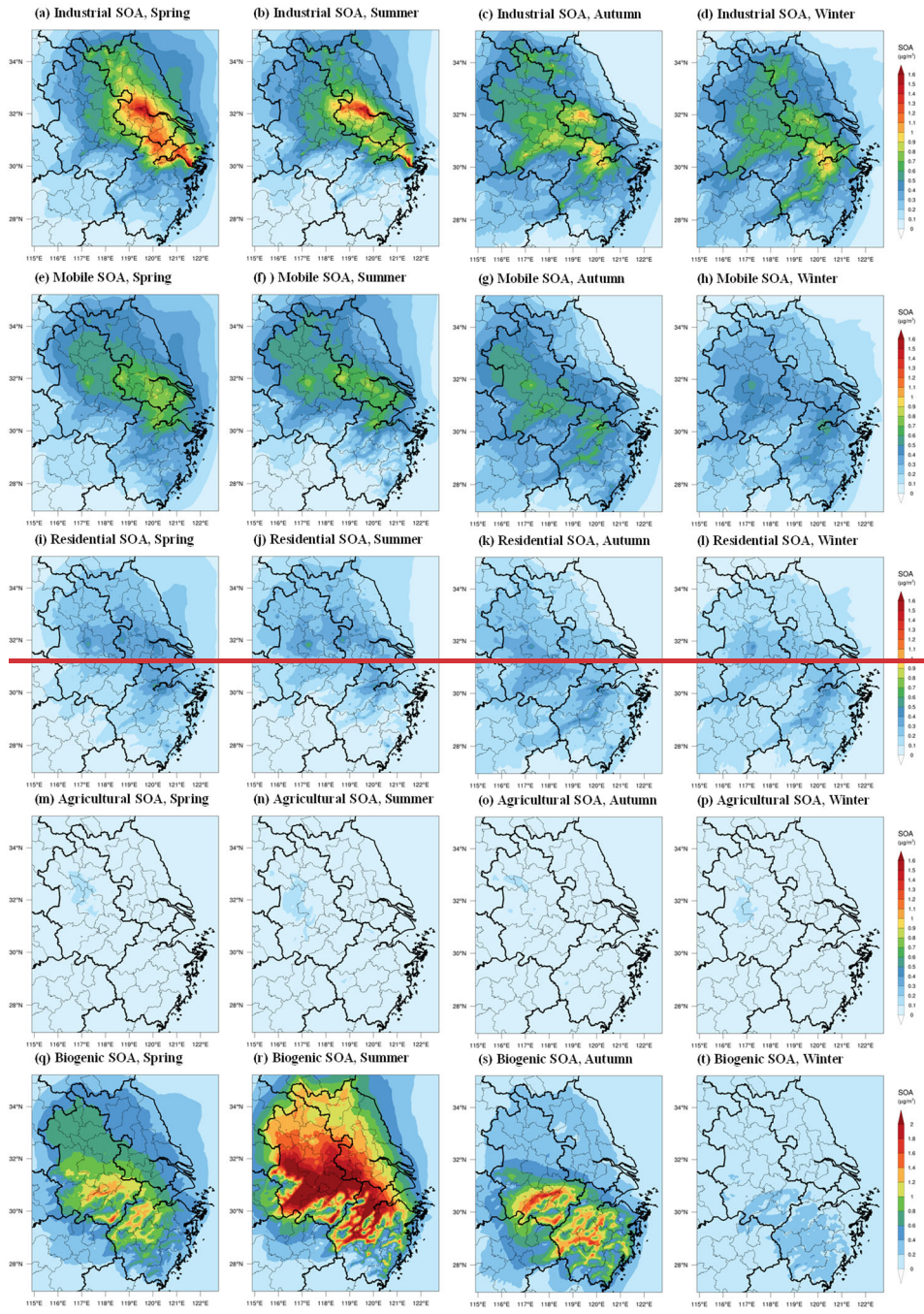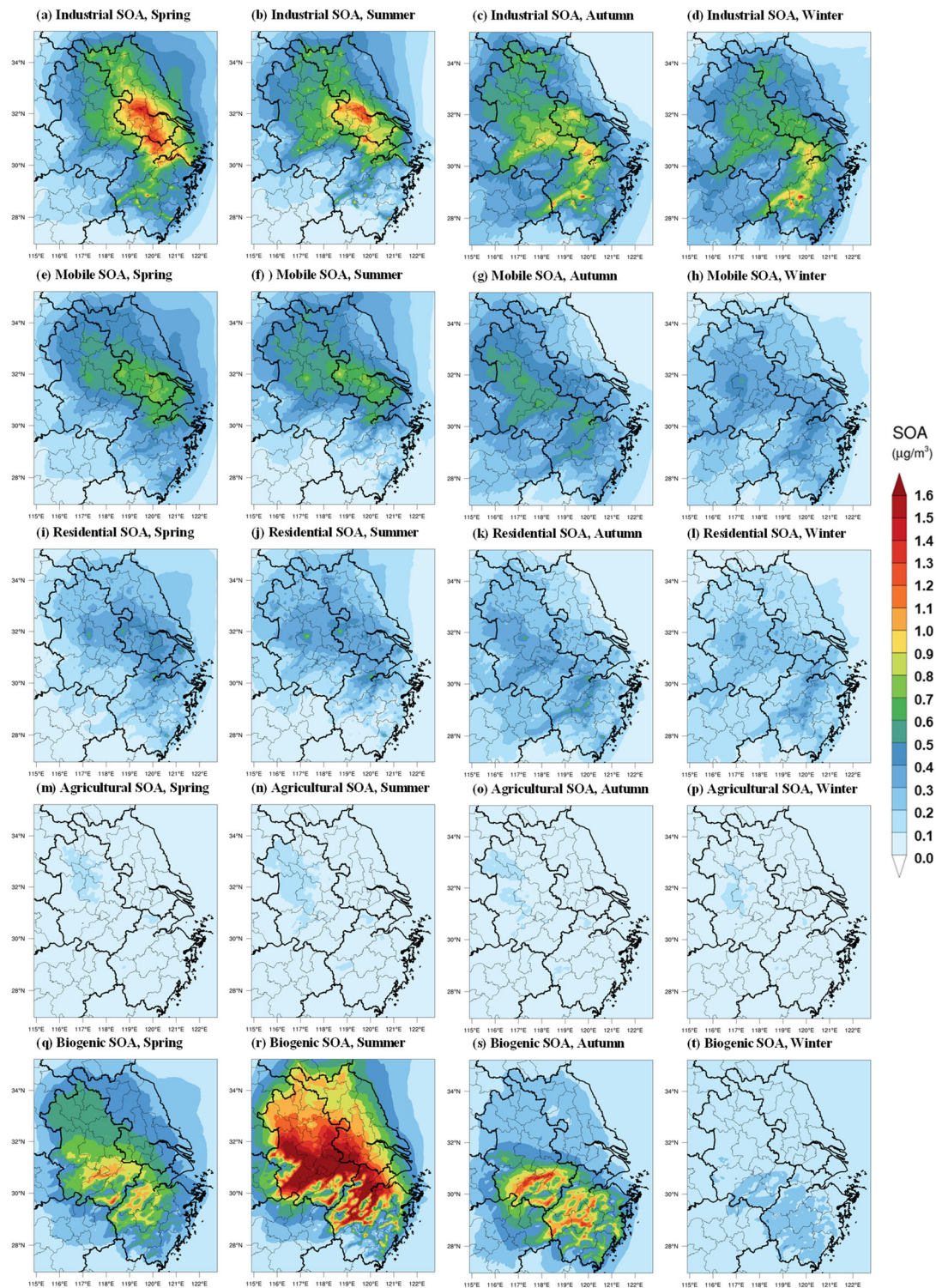
Figure 7~~7~~8. Spatial distributions of modeled SOA concentrations from different sources in each season in YRD region.

3.3.3 Predominant OA sources in sub-regions of YRD

To characterize the source contributions in different parts of the region, we categorized the simulation region into six sub-regions: northern YRD, western YRD,

750 central YRD, eastern YRD and southern YRD. And six representative cities in theses

751 six regions were further selected for detailed comparison in source contributions,

752 including Xuzhou (XZ), Hefei (HF), Nanjing (NJ), Hangzhou (HZ), Shanghai (SH) and

753 Jinhua (JH). Figure 8 shows their locations and OA source contributions during summer

754 and winter.

755 In Northern YRD, represented by XZ, enhanced contribution from super-regional

756 scale to the local OA was observed for both winter (64.6%~~53.2%~~) and summer

757 (27.7%~~28.9%~~) and the contributions from industrial processes (14.0%~~23.4%~~ in winter

758 and 21.0%~~18%~~ in summer) were also higher than other sub-regions. Other major

759 sources include biogenic (12.0%~~12.6%~~) and cooking emissions (14.1%~~14.7%~~) in

760 summer and cooking (14.1%~~9.3%~~) and other residential emissions (8.3%~~10.4%~~) in

761 winter. Taken together, supe-regional transportation and industrial processes are

762 predominant contributors of OA in northern YRD, accounting for 78.6% and 48.7%~~76.6%~~

763 ~~and 46.9%~~ in summer and winter respectively, followed by cooking emissions.

764 In western YRD, represented by HF, cooking emission was the largest contributor

765 to OA with contributions of 17.8% and 26.3%~~21.4% and 32.5%~~ in both summer and

766 winter respectively, followed by super-regional contributions of 15.7% ~~17.4%~~ (summer)

767 and 29.2%~~25.8%~~ (winter). Other major sources also include mobile source of

768 15.5%~~14%~~, biogenic source in summer (17.8%~~17.5%~~) and industrial processes in both

769 summer (12.3%~~12.6%~~) and winter (8.9%~~10.5%~~). In central YRD, represented by NJ

770 and HZ, the relative source contributions were very similar to those in western YRD,

771 with predominant contributions from cooking (22.8%-32.6%~~24.3%-38%~~), followed by

772 super-regional transportation (7.4%-31.8%~~8.8%-27.8%~~), industrial processes (11.3%-

773 18.4%~~10.9%-18.4%~~) and mobile source (13.1%-16.3%~~10%-13%~~).

774 In eastern YRD, represented by SH, the largest OA source was cooking emission,

775 account for 24.3%~~25.5%~~ and 36.6%~~43.6%~~ of OA in summer and winter respectively,

776 followed by mobile sources of 19%~~16%~~, super-regional transportation of 11.5%~~13.4~~%

777 (summer) and 22.2%~~25.8%~~ (winter) and industrial processes of 17.3%~~19.4%~~ (summer)

778 and 11.4%10.5% (winter). In southern YRD, represented by JH, while biogenic

779 contribution was prevailing in summer (38.2%37%), super-regional transportation was

780 significant in winter (31.8%28.7%). Similar to other sub-regions, other major sources

781 also included the contributions of cooking emission of 12.2%14.8% (summer) and

782 11.4%14.3% (winter), industrial processes of 12.9%8.7% (summer) and 117.9% 7.4%

783 (winter) and mobile sources of 13%. Yet southern YRD presented more evident increase

784 in the contribution from industrial solvent-use compared with other sub-regions.

785 To summarize, cooking, super-regional transportation, industrial process and mobile

786 sources were the predominant sources of OA in all sub-regions regardless of the season,

787 albeit enhanced contributions from biogenic sources to the OA formation in summer

788 was observed, especially in southern YRD. High contributions of cooking sources were

789 in accordance with the distributions of populations and high contributions of mobile

790 sources were somewhat expected, especially in the city centers. Source contributions of

791 OA varies in the intraregional scale implies that more targeted control measures need

792 to be designed according to the emission features of each city. Specifically, for densely

793 populated area, it is necessary to strengthen the future control strategy of cooking

794 emissions; special attention needs to be paid to the I/SVOC emissions from industrial

795 sources in eastern, central, and northern YRD region; mobile sources show its

796 significance in urban aera of the region, dominated by the equal contributions from

797 gasoline and diesel vehicles, indicating further reductions on the I/SVOCs from vehicle

798 emissions are therefore critical for pollution control on city scale.

(a) OA source contributions in summer
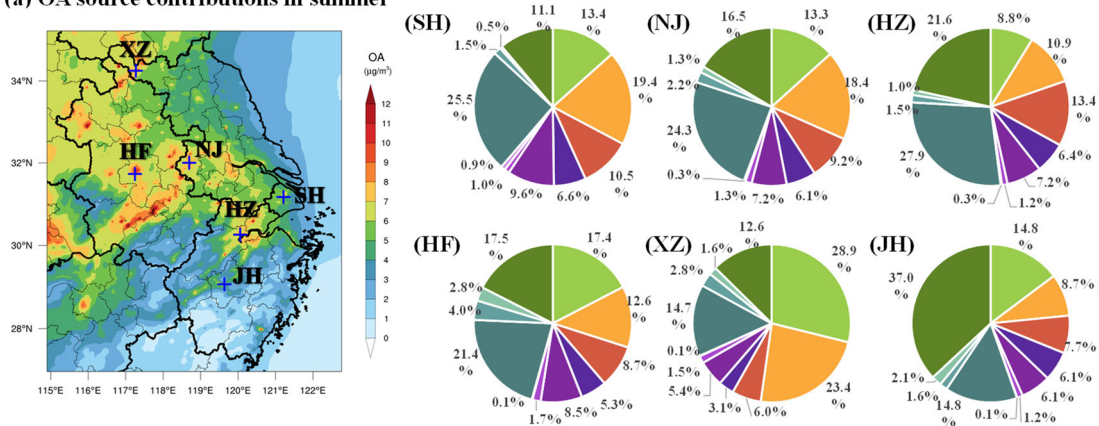
(b) OA source contributions in winter
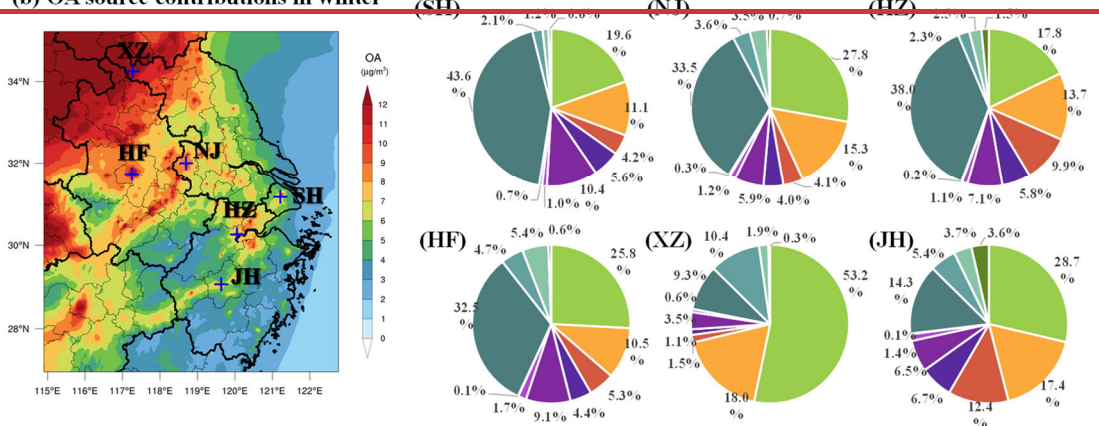
Super Region   **Industrial process**   **Industrial solvent-use**   **Gasoline vehicle**   **Diesel vehicle**
Diesel machinery   **Marine vessel**   **Cooking**   **Other Residential**   **Biomass burning**   **Biogenic**

799
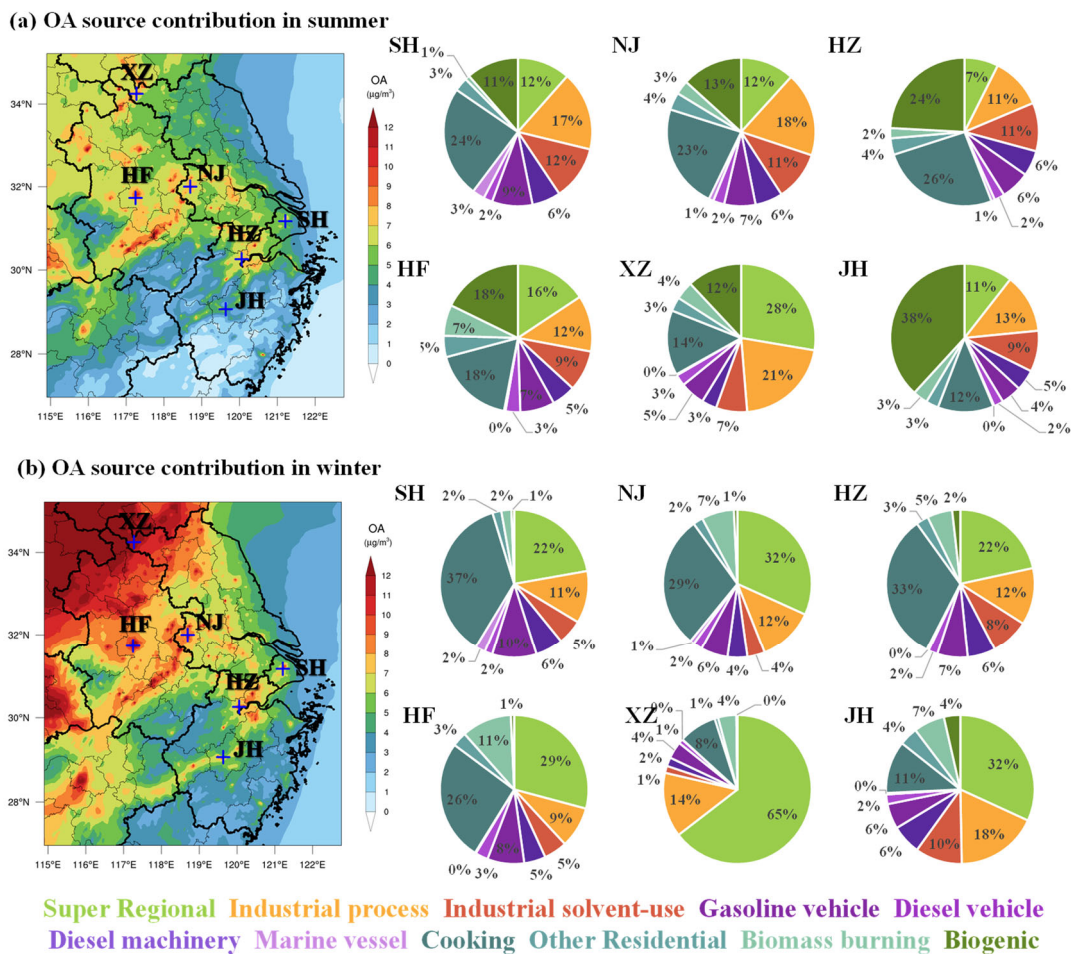
Figure 89. Source contributions of modeled OA concentrations from different sources during summer and winter in different cities of the region.

4. Conclusions

In this study, we established a high-resolution I/SVOC emission inventory with detailed source profiles and applied it into CMAQ v5.3 to simulate POA and SOA formation in YRD region of China. With the addition of I/SVOC emissions, simulation results show significant improvements on both temporal variations and spatial distributions of OA. Compared with the BASE simulation, where I/SVOC emissions were not included, the simulated SOA increased by 1.2 5 times in IMPROVE simulation, highlighting the significant contributions of I/SVOC emissions to SOA production. The remaining 10%−30%20% underestimation of OA indicates that future work is still needed in bridging the gap between simulation and observations, such as, measuring local emission factors and source profiles of I/SVOC from various local sources,

814   updating SOA formation mechanisms in model framework.

815   With the addition of source specific I/SVOC emissions, we successfully quantified

816   the contribution of each source to POA and SOA concentrations in YRD. For POA,

817   cooking emission is the predominant source, which concentrates in urban area of YRD

818   in accordance with the population distribution. For SOA, for the first time, we

819   demonstrate that I/SVOCs from industrial sources are dominant contributor, followed

820   by those from mobile sources. In summer, the contributions of biogenic emission to

821   total SOA are also non-negligible, especially for the cities in southern YRD. Spatial and

822   seasonal variations in the source contributions suggest that control strategies for OA

823   pollution should vary by cities and seasons. On regional scale, cooking emissions has

824   been emerging as an important POA source, not to mention their impacts on SOA

825   formation are not yet certain. Our results suggest the control measures on the cooking

826   emissions should be strengthened in the future for the further reduction of POA. We

827   also found that SOA in the region is primarily contributed by industrial I/SVOC

828   emissions, which urges in-depth studies of emission factors and source profiles of

829   I/SVOC emissions from industrial sources as well as the corresponding control

830   measures. On intraregional scale, for urban area, continuous reduction in I/SVOC

831   emissions from mobile sources, especially gasoline and diesel vehicles, are effective

832   measures in the mitigation of urban air pollution, which is also technically feasible as

833   has been demonstrated in Qi et al. (2021). Continuous improvement in emission

834   standards is one way to promote the reduction of motor vehicle related SOA.

835   *Data availability*

836   The gridded emissions of I/SVOCs from various sources for the YRD region

837   developed by this study at a horizontal resolution of 4 km × 4 km can be downloaded

838   from the following website (https://doi.org/10.6084/m9.figshare.19536082.v1).

839   Additional related data are available upon request by contacting the corresponding

840   author (Cheng Huang; huangc@saes.sh.cn).

841 *Supplement*

842   The supplement related to this article is available online.

843 *Author contributions*

844   CH, JA, DH, and MQ designed the research. CH and JA developed the I/SVOC

845 emission inventory. JA, MQ, and RY performed the model. DH, LQ, MZ, YL, SZ, and

846 QW collected the observation data. CH, JA, DH, and HW analyzed the results. CH, JA,

847 and DH wrote the paper.

848 *Competing interests*

849   The authors declare that they have no conflict of interest.

850 *Acknowledgement*

851   We thank the supports from the National Natural Science Foundation of China, the

852 Science and Technology Commission of the Shanghai Municipality, and the Shanghai

853 Municipal Bureau of Ecology and Environment.

854 *Financial support*

855   This work has been supported by the National Natural Science Foundation of

856 China (grant nos. 21777101), the Science and Technology Commission of the Shanghai

857 Municipality (grant no. 21230711000), the Shanghai Municipal Bureau of Ecology and

858 Environment Fund Project (grant no. 202001; 202114), and the State Environmental

859 Protection Key Laboratory of Formation and Prevention of Urban Air Pollution

860 Complex (grant no. CX2020080576).

861 **References**

862 An, J., Huang, Y., Huang, C., Wang, X., Yan, R., Wang, Q., Wang, H., Jing, S., Zhang, Y., Liu,

863   Y., Chen, Y., Xu, C., Qiao, L., Zhou, M., Zhu, S., Hu, Q., Lu, J., and Chen, C.: Emission

864   inventory of air pollutants and chemical speciation for specific anthropogenic sources

865   based on local measurements in the Yangtze River Delta region, China, Atmos. Chem.

866   Phys., 21, 2003–2025, 2021.

867 Boylan, J. W., and Russell, A. G.: PM and light extinction model performance metrics, goals,

868   and criteria for three-dimensional air quality models, Atmos. Environ., 40, 4946–4959,

869   2006.

870 Cai, S., Zhu, L., Wang, S., Wisthaler, A., Li, Q., Jiang, J., and Hao, J.: Time-resolved

871   intermediate-volatility and semivolatile organic compound emissions from household coal

872   combustion in northern China, Environ. Sci. Technol., 53, 9269−9278, 2019.

873 Canagaratna, M. R., Jayne, J. T., Jimenez, J. L., Allan, J. D., Alfarra, M. R., Zhang, Q., Onasch,

874   T. B., Drewnick, F., Coe, H., Middlebrook, A., Delia, A., Williams, L. R., Trimborn, A. M.,

875   Northway, M. J., DeCarlo, P. F., Kolb, C. E., Davidovits, P., and Worsnop, D. R.: Chemical

876   and microphysical characterization of ambient aerosols with the aerodyne aerosol mass

877   spectrometer, Mass Spectrom. Rev., 26, 185−222, 2007.

878 Canonaco, F., Crippa, M., Slowik, J. G., Baltensperger, U., and Prévôt, A. S. H.: SoFi, an IGOR-

879   based interface for the efficient use of the generalized multilinear engine (ME-2) for the

880   source apportionment: ME-2 application to aerosol mass spectrometer data, Atmos. Meas.

881   Tech., 6, 3649–3661, 2013.

882 Chang, X., Zhao, B., Zheng, H., Wang, S., Cai, S., Guo, F., Gui, P., Huang, G., Wu, D., Han, L.,

883   Xing, J., Man, H., Hu, R., Liang, C., Xu, Q., Qiu, X., Ding, D., Liu, K., Han, R., Robinson,

884   A. L., and Donahue, N. M.: Full-volatility emission framework corrects missing and

885   underestimated secondary organic aerosol sources, One Earth, 5, 403–412, 2022.

886 Chen, W., Ye, Y., Hu, W., Zhou, H., Pan, T., Wang, Y., Song, W., Song, Q., Ye, C., Wang, C.,

887   Wang, B., Huang, S., Yuan, B., Zhu, M., Lian, X., Zhang, G., Bi, X., Jiang, F., Liu, J.,

888   Canonaco, F., Prevot, A. S. H., Shao, M., and Wang, X.: Real-time characterization of

889   aerosol compositions, sources, and aging processes in Guangzhou during PRIDE-GBA

890   2018 campaign, J. Geophys. Res., Atmos., 126, e2021JD035114, 2021.

891 Crippa, M., Canonaco, F., Lanz, V. A., Äijälä, M., Allan, J. D., Carbone, S., Capes, G., Ceburnis,

892   D., Dall'Osto, M., Day, D. A., DeCarlo, P. F., Ehn, M., Eriksson, A., Freney, E.,

893   Hildebrandt Ruiz, L., Hillamo, R., Jimenez, J. L., Junninen, H., Kiendler-Scharr, A.,

894   Kortelainen, A. M., Kulmala, M., Laaksonen, A., Mensah, A. A., Mohr, C., Nemitz, E.,

895   O'Dowd, C., Ovadnevaite, J., Pandis, S. N., Petäjä, T., Poulain, L., Saarikoski, S., Sellegri,

896   K., Swietlicki, E., Tiitta, P., Worsnop, D. R., Baltensperger, U., and Prévôt, A. S. H.:

897   Organic aerosol components derived from 25 AMS data sets across Europe using a

898   consistent ME-2 based source apportionment approach, Atmos. Chem. Phys., 14, 6159–

899   6176, 2014.

900   Cross, E. S., Hunter, J. F., Carrasquillo, A. J., Franklin, J. P., Herndon, S. C., Jayne, J. T.,

901   Worsnop, D. R., Miake-Lye, R. C., and Kroll, J. H.: Online measurements of the emissions

902   of intermediate-volatility and semi-volatile organic compounds from aircraft, Atmos.

903   Chem. Phys., 13, 7845–7858, 2013.

904   Decker, Z. C. J., Robinson, M. A., Barsanti, K. C., Bourgeois, I., Coggon, M. M., DiGangi, J.

905   P., Diskin, G. S., Flocke, F. M., Franchin, A., Fredrickson, C. D., Gkatzelis, G. I., Hall, S.

906   R., Halliday, H., Holmes, C. D., Gregory Huey, L., Lee, Y. R., Lindaas, J., Middlebrook,

907   A. M., Montzka, D. D., Moore, R., Andrew Neuman, J., Nowak, J. B, Palm, B. B., Peischl,

908   J., Piel, F., Rickly, P. S., Rollins, A. W., Ryerson, T. B., Schwantes, R. H., Sekimoto, K.,

909   Thornhill, L., Thornton, J. A., Tyndall, G. S., Ullmann, K., Van Rooy, P., Veres, P. R.,

910   Warneke, C., Washenfelder, R. A., Weinheimer, A. J., Wiggins, E., Winstead, E., Wisthaler,

911   A., Womack, C., and Brown, S. S.: Nighttime and daytime dark oxidation chemistry in

912   wildfire plumes: an observation and model analysis of FIREX-AQ aircraft data, Atmos.

913   Chem. Phys., 21, 16293–16317, 2021.

914   Donahue, N. M., Robinson, A. L., and Pandis, S. N.: Atmospheric organic particulate matter:

915   From smoke to secondary organic aerosol, Atmos. Environ., 43, 94–106, 2009.

916   Donahue, N. M., Robinson, A. L., Stanier, C. O., and Pandis, S. N.: Coupled Partitioning,

917   Dilution, and Chemical Aging of Semivolatile Organics, Environ. Sci. Technol., 40, 2635–

918   2643, 2006.

919   Drozd, G. T., Weber, R. J., and Goldstein, A. H.: Highly resolved composition during diesel

920   evaporation with modeled ozone and secondary aerosol formation: Insights into pollutant

921   formation from evaporative intermediate volatility organic compound sources, Environ.

922   Sci. Technol., 55, 5742−5751, 2021.

923   Drozd, G. T., Zhao, Y., Saliba, G., Frodin, B., Maddox, C., Oliver Chang, M.-C., Maldonado,

924   H., Sardar, S., Weber, R. J., Robinson, A. L., and Goldstein, A. H.: Detailed speciation of

925   intermediate volatility and semivolatile organic compound emissions from gasoline

926   vehicles: Effects of cold-starts and implications for secondary organic aerosol formation,

927   Environ. Sci. Technol., 53, 1706–1714, 2019.

928   Emery, C., Tai, E., and Yarwood, G.: Enhanced meteorological modeling and performance

929   evaluation for two Texas ozone episodes, Prepared for the Texas natural resource

930   conservation commission, by ENVIRON International Corporation, 2001.

931   Gentner, D. R., Isaacman, G., Worton, D. R., Chan, A. W. H., Dallmann, T. R., Davis, L., Liu,

932   S., Day, D. A., Russell, L. M., Wilson, K. R., Weber, R., Guha, A., Harley, R. A., and

933   Goldstein, A. H.: Elucidating secondary organic aerosol from diesel and gasoline vehicles

934   through detailed characterization of organic carbon emissions, Proc. Natl. Acad. Sci., 109,

935   18318−18323, 2012.

936   Guo, J., Zhou, S., Cai, M., Zhao, J., Song, W., Zhao, W., Hu, W., Sun, Y., He, Y., Yang, C., Xu,

937   X., Zhang, Z., Cheng, P., Fan, Q., Hang, J., Fan, S., Wang, X., and Wang, X.:

938   Characterization of submicron particles by time-of-flight aerosol chemical speciation

939   monitor (ToF-ACSM) during wintertime: aerosol composition, sources, and chemical

940   processes in Guangzhou, China, Atmos. Chem. Phys., 20, 7595–7615, 2020.

941   Hallquist, M., Wenger, J. C., Baltensperger, U., Rudich, Y., Simpson, D., Claeys, M., Dommen,

942   J., Donahue, N. M., George, C., Goldstein, A. H., Hamilton, J. F., Herrmann, H., Hoffmann,

943   T., Iinuma, Y., Jang, M., Jenkin, M. E., Jimenez, J. L., Kiendler-Scharr, A., Maenhaut, W.,

944   McFiggans, G., Mentel, Th. F., Monod, A., Prévôt, A. S. H., Seinfeld, J. H., Surratt, J. D.,

945   Szmigielski, R., and Wildt, J.: The formation, properties and impact of secondary organic

946   aerosol: Current and emerging issues, Atmos. Chem. Phys., 9, 5155–5236, 2009.

947   Hayes, P. L., Ortega, A. M., Cubison, M. J., Froyd, K. D., Zhao, Y., Cliff, S. S., Hu, W. W.,

948   Toohey, D. W., Flynn, J. H., Lefer, B. L., Grossberg, N., Alvarez, S., Rappenglück, B.,

949   Taylor, J. W., Allan, J. D., Holloway, J. S., Gilman, J. B., Kuster, W. C., de Gouw, J. A.,

950   Massoli, P., Zhang, X., Liu, J., Weber, R. J., Corrigan, A. L., Russell, L. M., Isaacman, G.,

951   Worton, D. R., Kreisberg, N. M., Goldstein, A. H., Thalman, R., Waxman, E. M., Volkamer,

952   R., Lin, Y. H., Surratt, J. D., Kleindienst, T. E., Offenberg, J. H., Dusanter, S., Griffith, S.,

953   Stevens, P. S., Brioude, J., Angevine, W. M., and Jimenez, J. L.: Organic aerosol

954   composition and sources in Pasadena, California, during the 2010 CalNex campaign, J.

955   Geophys. Res., Atmos., 118, 9233–9257, 2013.

956   Huang, C., Hu, Q., Li, Y., Tian, J., Ma, Y., Zhao, Y., Feng, J., An, J., Qiao, L., Wang, H., Jing,

957   S., Huang, D., Lou, S., Zhou, M., Zhu, S., Tao, S., and Li, L.: Intermediate volatility

958   organic compound emissions from a large cargo vessel operated under real-world

959   conditions, Environ. Sci. Technol., 52, 12934–12942, 2018.

960   Huang, D., Zhu, S., An, J., Wang, Q., Qiao, L., Zhou, M., He, X., Ma, Y., Sun, Y., Huang, C.,

961   Yu, J., and Zhang, Q.: Comparative assessment of cooking emission contributions to urban

962   organic aerosol using online molecular tracers and aerosol mass spectrometry

963   measurements, Environ. Sci. Technol., 55, 14526–14535, 2021.

964   Huang, L., Wang, Q., Wang, Y., Emery, C., Zhu, A., Zhu, Y., Yin, S., Yarwood, G., Zhang, K.,

965   and Li, L.: Simulation of secondary organic aerosol over the Yangtze River Delta region:

966   The impacts from the emissions of intermediate volatility organic compounds and the SOA

967   modeling framework, Atmos. Environ., 246, 118079, 2021b.

968   Huang, R. J., Zhang, Y., Bozzetti, C., Ho, K., Cao, J., Han, Y., Daellenbach, K. R., Slowik, J.

969   G., Platt, S. M., Canonaco, F., Zotter, P., Wolf, R., Pieber, S. M., Bruns, E. A., Crippa, M.,

970   Ciarelli, G., Piazzalunga, A., Schwikowski, M., Abbaszade, G., Schnelle-Kreis, J.,

971   Zimmermann, R., An, Z., Szidat, S., Baltensperger, U., El Haddad, I., and Prévôt, A. S. H.:

972   High secondary aerosol contribution to particulate pollution during haze events in China,

973   Nature, 514, 218–222, 2014.

974   Huffman, J., Docherty, K., Mohr, C., Cubison, M., Ulbrich, I., Ziemann, P., Onasch, T., and

975   Jimenez, J.: Chemically-resolved volatility measurements of organic aerosol from

976   different sources, Environ. Sci. Technol., 43, 5351–5357, 2009.

977   Jathar, S. H., Gordon, T. D., Hennigan, C. J., Pye, H. O. T., Pouliot, G., Adams, P. J., Donahue,

978   N. M., and Robinson, A. L.: Unspeciated organic emissions from combustion sources and

979   their influence on the secondary organic aerosol budget in the United States, P. Natl. Acad.

980   Sci. USA, 111, 10473–10478, 2014.

981 Jathar, S. H., Woody, M., Pye, H. O. T., Baker, K. R., and Robinson, A. L.: Chemical transport

982   model simulations of organic aerosol in southern California: model evaluation and

983   gasoline and diesel source contributions, Atmos. Chem. Phys., 17, 4305–4318, 2017.

984 Jimenez, J. L., Canagaratna, M. R., Donahue, N. M., Prevot, A. S. H., Zhang, Q., Kroll, J. H.,

985   DeCarlo, P. F., Allan, J. D., Coe, H., Ng, N. L., Aiken, A. C., Docherty, K. S., Ulbrich, I.

986   M., Grieshop, A. P., Robinson, A. L., Duplissy, J., Smith, J. D., Wilson, K. R., Lanz, V. A.,

987   Hueglin, C., Sun, Y. L., Tian, J., Laaksonen, A., Raatikainen, T., Rautiainen, J., Vaattovaara,

988   P., Ehn, M., Kulmala, M., Tomlinson, J. M., Collins, D. R., Cubison, M. J., Dunlea, J.,

989   Huffman, J. A., Onasch, T. B., Alfarra, M. R., Williams, P. I., Bower, K., Kondo, Y.,

990   Schneider, J., Drewnick, F., Borrmann, S., Weimer, S., Demerjian, K., Salcedo, D., Cottrell,

991   L., Griffin, R., Takami, A., Miyoshi, T., Hatakeyama, S., Shimono, A., Sun, J. Y., Zhang,

992   Y. M., Dzepina, K., Kimmel, J. R., Sueper, D., Jayne, J. T., Herndon, S. C., Trimborn, A.

993   M., Williams, L. R., Wood, E. C., Middlebrook, A. M., Kolb, C. E., Baltensperger, U., and

994   Worsnop, D. R.: Evolution of Organic Aerosols in the Atmosphere, Science, 326, 1525–

995   1529, 2009.

996 Kim, D., Cho, C., Jeong, S., Lee, S., Nault, B. A., Campuzano-Jost, P., Day, D. A., Schroder, J.

997   C., Jimenez, J. L., Volkamer, R., Blake, D. R., Wisthaler, A., Fried, A., DiGangi, J. P.,

998   Diskin, G. S., Pusede, S. E., Hall, S. R., Ullmann, K., Gregory Huey, L., Tanner, D. J.,

999   Dibb, J., Knote, C. J., and Min, K., Field observational constraints on the controllers in

1000   glyoxal (CHOCHO) reactive uptake to aerosol, Atmos. Chem. Phys., 22, 805–821, 2022.

1001 Koo, B., Knipping, E., and Yarwood, G.: 1.5-Dimensional volatility basis set approach for

1002   modeling organic aerosol in CAMx and CMAQ, Atmos. Environ., 95, 158–164, 2014.

1003 Koss, A. R., Sekimoto, K., Gilman, J. B., Selimovic, V., Coggon, M. M., Zarzana, K. J., Yuan,

1004   B., Lerner, B. M., Brown, S. S., Jimenez, J. L., Krechmer, J., Roberts, J. M., Warneke, C.,

1005   Yokelson, R. J., and de Gouw, J.: Non-methane organic gas emissions from biomass

1006   burning: identification, quantification, and emission factors from PTR-ToF during the

1007   FIREX 2016 laboratory experiment, Atmos. Chem. Phys., 18, 3299–3319, 2018.

Li, J., Cao, L., Gao, W., He, L., Yan, Y., He, Y., Pan, Y., Ji, D., Liu, Z., and Wang, Y.: Seasonal variations in the highly time-resolved aerosol composition, sources and chemical processes of background submicron particles in the North China Plain, Atmos. Chem. Phys., 21, 4521–4539, 2021.

Li, J., Han, Z., Li, J., Liu, R., Wu, Y., Liang, L., and Zhang, R.: The formation and evolution of secondary organic aerosol during haze events in Beijing in wintertime, Sci. Total Environ., 703, 134937, 2020.

Li, J., Han, Z., Wu, J., Tao, J., Li, J., Sun, Y., Liang, L., Liang, M., and Wang, Q.: Secondary organic aerosol formation and source contributions over east China in summertime, Environ. Pollut., 306, 119383, 2022.

Li, M., Zhang, Q., Kurokawa, J. i., Woo, J. H., He, K., Lu, Z., Ohara, T., Song, Y., Streets, D. G., Carmichael, G. R., Cheng, Y., Hong, C., Huo, H., Jiang, X., Kang, S., Liu, F., Su, H., Zheng, B.: MIX: a mosaic Asian anthropogenic emission inventory under the international collaboration framework of the MICS-Asia and HTAP. Atmos. Chem. Phys., 17, 935–963, 2017.

Li, Y., Ren, B., Qiao, Z., Zhu, J., Wang, H., Zhou, M., Qiao, L., Lou, S., Jing, S., Huang, C., Tao, S., Rao, P., and Li, J.: Characteristics of atmospheric intermediate volatility organic compounds (IVOCs) in winter and summer under different air pollution levels, Atmos. Environ., 210, 58–65, 2019.

Li, Y. J., Sun, Y. L., Zhang, Q., Li, X., Li, M., Zhou, Z., and Chan, C. K.: Real-time chemical characterization of atmospheric particulate matter in China: A review, Atmos. Environ., 158, 270–304, 2017.

Liggio, J., Li, S., Hayden, K., Taha, Y. M., Stroud, C., Darlington, A., Drollette, B. D., Gordon, M., Lee, P., Liu, P., Leithead, A., Moussa, S. G., Wang, D., Brien, J. O., Mittermeier, R. L., Osthoff, H. D., Makar, P. A., Zhang, J., Brook, J. R., Lu, G., Staebler, R. M., Han, Y., Travis, W., Plata, D. L., and Gentner, D. R.: Oil sands operations as a large source of secondary organic aerosols, Nature, 534, 1–16, 2016.

Ling, Z., Wu, L., Wang, Y., Shao, M., Wang, X., and Huang, W.: Roles of semivolatile and

intermediate-volatility organic compounds in secondary organic aerosol formation and its implication: A review, J. Environ. Sci., 114, 259–285, 2022.

Lim, Y. B. and Ziemann, P. J.: Chemistry of secondary organic aerosol formation from OH radical-initiated reactions of linear, branched, and cyclic alkanes in the presence of NO_x, Aerosol Sci. Technol., 43, 604–619, 2009.

Liu, H., Man, H., Cui, H., Wang, Y., Deng, F., Wang, Y., Yang, X., Xiao, Q., Zhang, Q., Ding, Y., and He, K.: An updated emission inventory of vehicular VOCs and IVOCs in China, Atmos. Chem. Phys., 17, 12709–12724, 2017.

Liu, H., Meng, Z., Lv, Z., Wang, X., Deng, F., Liu, Y., Zhang, Y., Shi, M., Zhang, Q., and He, K.: Emissions and health impacts from global shipping embodied in US–China bilateral trade, Nat. Sustain., 2, 1027–1033, 2019.

Liu, Y., Li, L., An, J., Huang, L., Yan, R., Huang, C., Wang, H., Wang, Q., Wang, M., and Zhang, W.: Estimation of biogenic VOC emissions and its impact on ozone formation over the Yangtze River Delta region, China, Atmos. Environ., 186, 113–128, 2018a.

Liu, Z., Gao, W., Yu, Y., Hu, B., Xin, J., Sun, Y., Wang, L., Wang, G., Bi, X., Zhang, G., Xu, H., Cong, Z., He, J., Xu, J., and Wang, Y.: Characteristics of PM2.5 mass concentrations and chemical species in urban and background areas of China: emerging results from the CARE-China network, Atmos. Chem. Phys., 18, 8849–8871, 2018.

Louvaris, E. E., Florou, K., Karnezi, E., Papanastasiou, D. K., Gkatzelis, G. I., and Pandis, S. N.: Volatility of source apportioned wintertime organic aerosol in the city of Athens, Atmos. Environ., 158, 138–147, 2017.

Lu, Q., Murphy, B. N., Qin, M., Adams, P. J., Zhao, Y., Pye, H. O. T., Efstathiou, C., Allen, C., and Robinson, A. L.: Simulation of organic aerosol formation during the CalNex study: Updated mobile emissions and secondary organic aerosol parameterization for intermediate-volatility organic compounds, Atmos. Chem. Phys., 20, 4313–4332, 2020.

Lu, Q., Zhao, Y., and Robinson, A. L.: Comprehensive organic emission profiles for gasoline, diesel, and gas-turbine engines including intermediate and semi-volatile organic compound emissions, Atmos. Chem. Phys., 18, 17637–17654, 2018.

1064   May, A. A., Levin, E. J. T., Hennigan, C. J., Riipinen, I., Lee, T., Collett, J. L., Jimenez, J. L.,

1065   Kreidenweis, S. M., and Robinson, A. L.: Gas-particle partitioning of primary organic

1066   aerosol emissions: 3. Biomass burning, J. Geophys. Res.-Atmos., 118, 11327–11338, 2013.

1067   McDonald, B. C., de Gouw, J. A., Gilman, J. B., Jathar, S. H., Akherati, A., Cappa, C. D.,

1068   Jimenez, J. L., Lee-Taylor, J., Hayes, P. L., McKeen, S. A., Cui, Y. Y., Kim, S., Gentner,

1069   D. R., Isaacman-VanWertz, G., Goldstein, A. H., Harley, R. A., Frost, G. J., Roberts, J. M.,

1070   Ryerson, T. B., and Trainer, M.: Volatile chemical products emerging as largest

1071   petrochemical source of urban organic emissions, Science, 359, 760–764, 2018.

1072   Miao, R., Chen, Q., Shrivastava, M., Chen, Y., Zhang, L., Hu, J., Zheng, Y., and Liao, K.:

1073   Process-based and observation-constrained SOA simulations in China: the role of

1074   semivolatile and intermediate-volatility organic compounds and OH levels, Atmos. Chem.

1075   Phys., 21, 16183–16201, 2021.

1076   Ming, L., Jin, L., Li, J., Fu, P., Yang, W., Liu, D., Zhang, G., Wang, Z., and Li, X.: $PM_{2.5}$ in the

1077   Yangtze River Delta, China: Chemical compositions, seasonal variations, and regional

1078   pollution events, Environ. Pollut., 223, 200–212, 2017.

1079   Murphy, B. N., Woody, M. C., Jimenez, J. L., Carlton, A. M. G., Hayes, P. L., Liu, S., Ng, N.

1080   L., Russell, L. M., Setyan, A., and Xu, L.: Semivolatile POA and parameterized total

1081   combustion SOA in CMAQv5.2: impacts on source strength and partitioning, Atmos.

1082   Chem. Phys., 17, 11107–11133, 2017.

1083   Nault, B. A., Jo, D. S., McDonald, B. C., Campuzano-Jost, P., Day, D. A., Hu, W., Schroder, J.

1084   C., Allan, J., Blake, D. R., Canagaratna, M. R., Coe, H., Coggon, M. M., DeCarlo, P. F.,

1085   Diskin, G. S., Dunmore, R., Flocke, F., Fried, A., Gilman, J. B., Gkatzelis, G., Hamilton,

1086   J. F., Hanisco, T. F., Hayes, P. L., Henze, D. K., Hodzic, A., Hopkins, J., Hu, M., Huey, L.

1087   G., Jobson, B. T., Kuster, W. C., Lewis, A., Li, M., Liao, J., Nawaz, M. O., Pollack, I. B.,

1088   Peischl, J., Rappenglück, B., Reeves, C. E., Richter, D., Roberts, J. M., Ryerson, T. B.,

1089   Shao, M., Sommers, J. M., Walega, J., Warneke, C., Weibring, P., Wolfe, G. M., Young, D.

1090   E., Yuan, B., Zhang, Q., de Gouw, J. A., and Jimenez, J. L.: Secondary organic aerosols

1091   from anthropogenic volatile organic compounds contribute substantially to air pollution

mortality, Atmos. Chem. Phys., 21, 11201–11224, 2021.

Presto, A. A., Miracolo, M. A., Kroll, J. H., Worsnop, D. R., Robinson, A. L., and Donahue, N. M.: Intermediate-volatility organic compounds: A potential source of ambient oxidized organic aerosol, Environ. Sci. Technol., 43, 4744–4749, 2009.

~~Presto, A. A., Miracolo, M. A., Donahue, N. M., and Robinson, A. L.: Secondary organic aerosol formation from high-NO$_x$ photo-oxidation of low volatility precursors: n-alkanes, Environ. Sci. Technol., 44, 2029–2034, 2010.~~

Presto, A. A., Nguyen, N. T., Ranjan, M., Reeder, A. J., Lipsky, E. M., Hennigan, C. J., Miracolo, M. A., Riemer, D. D., and Robinson, A. L.: Fine particle and organic vapor emissions from staged tests of an in-use aircraft engine, Atmos. Environ., 45, 3603–3612, 2011.

Qi, L., Liu, H., Shen, X., Fu, M., Huang, F., Man, H., Deng, F., Shaikh, A. A., Wang, X., Dong, R., Song, C., and He, K.: Intermediate-volatility organic compound emissions from nonroad construction machinery under different operation modes, Environ. Sci. Technol., 53, 13832–13840, 2019.

Qi, L., Zhao, J., Li, Q., Su, S., Lai, Y., Deng, F., Man, H., Wang, X., Shen, X., Lin, Y., Ding, Y., and Liu, H.: Primary organic gas emissions from gasoline vehicles in China: Factors, composition and trends, Environ. Pollut., 290, 117984, 2021.

Qin, M., Hu, A., Mao, J., Li, X., Sheng, L., Sun, J., Li, J., Wang, X., Zhang, Y., Hu, J.: PM$_{2.5}$ and O$_3$ relationships affected by the atmospheric oxidizing capacity in the Yangtze River Delta, China, Sci. Total Environ., 810, 152268, 2022.

Ren, B., Zhu, J., Tian, L., Wang, H., Huang, C., Jing, S., Lou, S., An, J., Lu, J., Rao, P., Fu, Q., Huo, J., and Li, Y.: An alternative semi-quantitative GC/MS method to estimate levels of airborne intermediate volatile organic compounds (IVOCs) in ambient air, Atmos. Environ., X6, 100075, 2020.

Robinson, A. L., Donahue, N. M., Shrivastava, M. K., Weitkamp, E. A., Sage, A. M., Grieshop, A. P., Lane, T. E., Pierce, J. R., and Pandis, S. N.: Rethinking organic aerosols: Semivolatile emissions and photochemical aging, Science, 315, 1259–1262, 2007.

Sartelet, K., Zhu, S., Moukhtar, S., André, M., Gros, V., Favez, O., Brasseurh, A., and Redaelli,

M.: Emission of intermediate, semi and low volatile organic compounds from traffic and their impact on secondary organic aerosol concentrations over greater paris, Atmos. Environ, 180, 126–137, 2018.

Shrivastava, M. K., Cappa, C. D., Fan, J., Goldstein, A. H., Guenther, A. B., Jimenez, J. L., Kuang, C., Laskin, A., Martin, S. T., Ng, N. L., Petaja, T., Pierce, J. R., Rasch, P. J., Roldin, P., Seinfeld, J. H., Shilling, J., Smith, J. N., Thornton, J. A., Volkamer, R., Wang, J., Worsnop, D. R., Zaveri, R. A., Zelenyuk, A., and Zhang, Q.: Recent advances in understanding secondary organic aerosol: Implications for global climate forcing, Rev. Geophys., 55, 509–559, 2017.

Shrivastava, M., Fast, J., Easter, R., Gustafson, W. I., Zaveri, R. A., Jimenez, J. L., Saide, P., and Hodzic, A.: Modeling organic aerosols in a megacity: comparison of simple and complex representations of the volatility basis set approach, Atmos. Chem. Phys., 11, 6639–6662, 2011.

Sun, Y., Jiang, Q., Wang, Z., Fu, P., Li, J., Yang, T., and Yin, Y.: Investigation of the sources and evolution processes of severe haze pollution in Beijing in January 2013, J. Geophys. Res., Atmos., 119, 4380–4398, 2014.

Tang, J., Li, Y., Li, X., Jing, S., Huang, C., Zhu, J., Hu, Q., Wang, H., Lu, J., Lou, S., Rao, P., and Huang, D.: Intermediate volatile organic compounds emissions from vehicles under real world conditions, Sci. Total Environ., 788, 147795, 2021.

Tao, J., Zhang, L., Cao, J., and Zhang, R.: A review of current knowledge concerning $PM_{2.5}$ chemical composition, aerosol optical properties and their relationships across China, Atmos. Chem. Phys., 17, 9485–9518, 2017.

Tkacik, D. S., Presto, A. A., Donahue, N. M., and Robinson, A. L.: Secondary organic aerosol formation from intermediate-volatility organic compounds: Cyclic, linear, and branched alkanes, Environ. Sci. Technol., 46, 8773–8781, 2012.

Tsimpidi, A. P., Karydis, V. A., Zavala, M., Lei, W., Molina, L., Ulbrich, I. M., Jimenez, J. L., and Pandis, S. N.: Evaluation of the volatility basis-set approach for the simulation of organic aerosol formation in the Mexico City metropolitan area, Atmos. Chem. Phys., 10,

525–546, 2010.

US EPA: Final Report, SPECIATE Version 5.1, Database Development Documentation, available at: https://www.epa.gov/air-emissions-modeling/speciate-51-and-50-addendum-and-final-report (last access: 8 August 2021), 2021

Woody, M. C., Baker, K. R., Hayes, P. L., Jimenez, J. L., Koo, B., and Pye, H. O. T.: Understanding sources of organic aerosol during CalNex-2010 using the CMAQ-VBS, Atmos. Chem. Phys., 16, 4081–4100, 2016.

Wu, L., Ling, Z., Liu, H., Shao, M., Lu, S., Wu, L., and Wang, X.: A gridded emission inventory of semi-volatile and intermediate volatility organic compounds in China, Sci. Total Environ., 761, 143295, 2021.

Wu, L., Wang, X., Lu, S., Shao, M., and Ling, Z.: Emission inventory of semi-volatile and intermediate-volatility organic compounds and their effects on secondary organic aerosol over the Pearl River Delta region, Atmos. Chem. Phys., 19, 8141–8161, 2019.

Xu, L., Guo, H., Boyd, C. M., Klein, M., Bougiatioti, A., Cerully, K. M., Hite, J. R., Isaacman-VanWertze, G., Kreisberg, N. M., Knote, C., Olson, K., Koss, A., Goldstein, A. H., Hering, S. V., de Gouw, J., Baumann, K., Lee, S., Nenes, A., Weber, R. J., and Ng, N. L.: Effects of anthropogenic emissions on aerosol formation from isoprene and monoterpenes in the southeastern United States, P. Natl. Acad. Sci. USA, 112, 37–42, 2015.

Yang, W., Li, J., Wang, W., Li, J., Ge, M., Sun, Y., Chen, X., Ge, B., Tong, S., Wang, Q., and Wang, Z.: Investigating secondary organic aerosol formation pathways in China during 2014, Atmos. Environ., 213, 133–147, 2019.

Yao, T., Li, Y., Gao, J., Fung, J. C. H., Wang, S., Li, Y., Chan, C. K., and Lau, A. K. H.: Source apportionment of secondary organic aerosols in the Pearl River Delta region: Contribution from the oxidation of semi-volatile and intermediate volatility primary organic aerosols, Atmos. Environ., 222, 117111, 2020.

Yu, K., Zhu, Q., Du, K., and Huang, X.: Characterization of nighttime formation of particulate organic nitrates based on high-resolution aerosol mass spectrometry in an urban atmosphere in China, Atmos. Chem. Phys., 19, 5235–5249, 2019.

1176 Yuan, B., Shao, M., Lu, S., and Wang, B.: Source profiles of volatile organic compounds
1177   associated with solvent use in Beijing, China, Atmos. Environ., 44, 1919–1926, 2010.

1178 Zhang, H, Yee, L. D., Lee, B. H., Curtis, M. P., Worton, D. R., Isaacman-VanWertz, G.,
1179   Offenberg, J. H., Lewandowski, M., Kleindienst, T. E., Beaver, M. R., Holder, A. L.,
1180   Lonneman, W. A., Docherty, K. S., Jaoui, M., Pye, H. T. O., Hu, W., Day, D. A.,
1181   Campuzano-Jost, P., Jimenez, J. L., Guo, H., Weber, R. J., de Gouw, J., Koss, A. R.,
1182   Edgerton, E. S., Brune, W., Mohr, C., Lopez-Hilfiker, F. D., Lutz, A., Kreisberg, N. M.,
1183   Spielman, S. R., Hering, S. V., Wilson, K. R., Thornton, J. A., and Goldstein, A. H.:
1184   Monoterpenes are the largest source of summertime organic aerosol in the southeastern
1185   United States, P. Natl. Acad. Sci. USA, 115, 2038–2043, 2018.

1186 Zhang, Q., Jimenez, J. L., Canagaratna, M. R., Allan, J. D., Coe, H., Ulbrich, I., Alfarra, M. R.,
1187   Takami, A., Middlebrook, A. M., Sun, Y. L., Dzepina, K., Dunlea, E., Docherty, K.,
1188   DeCarlo, P. F., Salcedo, D., Onasch, T., Jayne, J. T., Miyoshi, T., Shimono, A., Hatakeyama,
1189   S., Takegawa, N., Kondo, Y., Schneider, J., Drewnick, F., Borrmann, S., Weimer, S.,
1190   Demerjian, K., Williams, P., Bower, K., Bahreini, R., Cottrell, L., Griffin, R. J., Rautiainen,
1191   J., Sun, J. Y., Zhang, Y. M., and Worsnop, D. R.: Ubiquity and dominance of oxygenated
1192   species in organic aerosols in anthropogenically-influenced Northern Hemisphere
1193   midlatitudes, Geophys. Res. Lett., 34, L13801, 2007.

1194 Zhang, Q., Jimenez, J. L., Canagaratna, M. R., Ulbrich, I. M., Ng, N. L., Worsnop, D. R., and
1195   Sun, Y.: Understanding atmospheric organic aerosols via factor analysis of aerosol mass
1196   spectrometry: a review, Anal. Bioanal. Chem., 401, 3045−3067, 2011.

1197 Zhang, Y., Vijayaraghavan, K., and Seigneur, C.: Evaluation of three probing techniques in a
1198   three-dimensional air quality model, J. Geophys. Res., Atmos., 110, D02305, 2005.

1199 Zhao, B., Wang, S., Donahue, N. M., Jathar, S. H., Huang, X. F., Wu, W., Hao, J., and Robinson,
1200   A. L.: Quantifying the effect of organic aerosol aging and intermediate-volatility emissions
1201   on regional scale aerosol pollution in China, Sci. Rep., 6, 28815, 2016a.

1202 Zhao, Y., Hennigan, C. J., May, A. A., Tkacik, D. S., De Gouw, J. A., Gilman, J. B., Kuster, W.
1203   C., Borbon, A., and Robinson, A. L.: Intermediate-volatility organic compounds: A large

1204   source of secondary organic aerosol, Environ. Sci. Technol., 48, 13743–13750, 2014.

1205   Zhao, Y., Kreisberg, N. M., Worton, D. R., Isaacman, G., Weber, R. J., Liu, S., Day, D. A.,

1206   Russell, L. M., Markovic, M. Z., VandenBoer, T. C., Murphy, J. G., Hering, S. V., and

1207   Goldstein, A. H.: Insights into secondary organic aerosol formation mechanisms from

1208   measured gas/particle partitioning of specific organic tracer compounds, Environ. Sci.

1209   Technol., 47, 3781−3787, 2013.

1210   Zhao, Y., Nguyen, N. T., Presto, A. A., Hennigan, C. J., May, A. A., and Robinson, A. L.:

1211   Intermediate volatility organic compound emissions from on-road diesel vehicles:

1212   Chemical composition, emission Factors, and estimated secondary organic aerosol

1213   production, Environ. Sci. Technol., 49, 11516–11526, 2015.

1214   Zhao, Y., Nguyen, N. T., Presto, A. A., Hennigan, C. J., May, A. A., and Robinson, A. L.:

1215   Intermediate Volatility Organic Compound Emissions from On-Road Gasoline Vehicles

1216   and Small Off-Road Gasoline Engines, Environ. Sci. Technol., 50, 4554–4563, 2016b.

1217   Zheng, M., Cass, G. R., Schauer, J. J., and Edgerton, E. S.: Source Apportionment of $PM_{2.5}$ in

1218   the Southeastern United States Using Solvent-Extractable Organic Compounds as Tracers,

1219   Environ. Sci. Technol., 36, 2361−2371, 2002.

1220   Zhu, S., Wang, Q., Qiao, L., Zhou, M., Wang, S., Lou, S., Huang, D., Wang, Q., Jing, S., Wang,

1221   H., Chen, C., Huang, C., and Yu, J. Z.: Tracer-based characterization of source variations

1222   of $PM_{2.5}$ and organic carbon in Shanghai influenced by the COVID-19 lockdown, Faraday

1223   Discuss., 226, 112, 2021.

1224   Zhu, W., Zhou, M., Cheng, Z., Yan, N., Huang, C., Qiao, L., Wang, H., Liu, Y., Lou, S., and

1225   Guo, S.: Seasonal variation of aerosol compositions in Shanghai, China: Insights from

1226   particle aerosol mass spectrometer observations, Sci. Total Environ., 771, 144948, 2021.

1227